

1 **Ironomycin induces mantle cell lymphoma cell death by targeting iron metabolism addiction**

2 Sara Ovejero<sup>1,2,#</sup>, Laura Alibert<sup>1,2,#</sup>, Julie Devin<sup>1,2</sup>, Tatiana Cañeque<sup>3</sup>, Valentin Jacquier<sup>1,2</sup>, Andrea Romero<sup>1,2</sup>,  
3 Salome Amar<sup>1,2</sup>, Matthieu Abouladze<sup>2</sup>, Elvira Garcia de Paco<sup>2</sup>, Ouissem Karmous Gadacha<sup>2</sup>, Guilhem  
4 Requirand<sup>2</sup>, Nicolas Robert<sup>2</sup>, Miss Lერიem Zellagui<sup>1</sup>, Hugues de Bousac<sup>4</sup>, Guillaume Cartron<sup>5,6</sup>, Johanna  
5 Chiche<sup>8,9</sup>, Jean-Ehrland Ricci<sup>8,9</sup>, Charles Herbaux<sup>1,6,7</sup>, Raphael Rodriguez<sup>3</sup>, Jerome Moreaux<sup>1,2,6,7\*</sup> and  
6 Caroline Bret<sup>1,2,6\*</sup>

7 **Affiliations**

8 1. Institute of Human Genetics UMR 9002 CNRS-UM, Montpellier, France  
9 2. Department of Biological Hematology, CHU Montpellier, Montpellier, France  
10 3. Chemical Biology of Cancer Laboratory, Institut Curie, 26 rue d'Ulm, 75248 Paris Cedex 05, France; PSL  
11 Université, Paris, France; CNRS UMR 3666, Paris, France; INSERM U1143, Paris, France  
12 4. Diag2Tec, Montpellier, France  
13 5. Department of Clinical Hematology, CHU Montpellier, Montpellier, France  
14 6. UFR Médecine, University of Montpellier, Montpellier, France  
15 7. Institut Universitaire de France, Paris, France  
16 8. Université Côte d'Azur, INSERM, C3M, Nice, France,  
17 9. Équipe labellisée LIGUE Contre le Cancer, Nice, France  
18 # Co-first authors: The authors contributed equally.  
19 \* Corresponding authors. The authors contributed equally.  
20

21 **Corresponding Authors:**

22 Dr Caroline Bret  
23 Department of Biological Hematology  
24 Hôpital Saint-Eloi - CHRU de Montpellier  
25 80, av. Augustin Fliche  
26 34295 Montpellier Cedex 5  
27 IGH - Institute of Human Genetics  
28 CNRS UMR-UM 9002  
29 <http://www.igh.cnrs.fr>  
30 phone: +33 (0)4 67 33 70 31  
31 fax: +33 (0)4 67 33 70 36  
32 mail: [c-bret@chu-montpellier.fr](mailto:c-bret@chu-montpellier.fr)  
33

34 Pr Jérôme Moreaux  
35 Laboratory for Monitoring Innovative Therapies  
36 Department of Biological Hematology  
37 Hôpital Saint-Eloi - CHRU de Montpellier  
38 80, av. Augustin Fliche  
39 34295 Montpellier Cedex 5  
40 IGH - Institute of Human Genetics  
41 CNRS UMR-UM 9002  
42 <http://www.igh.cnrs.fr>  
43 fax: +33 (0)4 67 33 70 36  
44 mail: [jerome.moreaux@igh.cnrs.fr](mailto:jerome.moreaux@igh.cnrs.fr)  
45

46 **Data sharing statement:**

47 For original data, please contact [c-bret@chu-montpellier.fr](mailto:c-bret@chu-montpellier.fr) and [jerome.moreaux@igh.cnrs.fr](mailto:jerome.moreaux@igh.cnrs.fr)

48 The genomic data are available at Gene Expression Omnibus repository under the accession number  
49 GSE273121.

50

51 **Key Points:**

52 1/ Iron homeostasis represents a potential therapeutic target for patients with MCL that can be  
53 targeted with ironomycin.

54

55 2/ Ironomycin induces dysregulation of BCR pathway in MCL cells and synergizes with BTK inhibitor.

56

57 **Abstract**

58 Rationale: Mantle-cell lymphoma (MCL) remains an aggressive and incurable cancer. Accumulating  
59 evidence reveals that abnormal iron metabolism plays an important role in tumorigenesis and in cancer  
60 progression of many tumors. Based on these data, we searched to identify alterations of iron homeostasis  
61 in MCL that could be exploited to develop novel therapeutic strategies.

62 Methods: Analysis of the iron metabolism gene expression profile of a cohort of patients with MCL enables  
63 the identification of patients with a poor outcome who might benefit from an iron homeostasis-targeted  
64 therapy. We analyzed the therapeutic interest of ironomycin, known to sequester iron in the lysosome  
65 and to induce ferroptosis.

66 Results: In a panel of MCL cell lines, ironomycin inhibited MCL cell growth at nanomolar concentrations  
67 compared with conventional iron chelators. Ironomycin treatment resulted in ferroptosis induction and  
68 decreased cell proliferation rate, with a reduced percentage of cells in S-phase together with Ki67 and  
69 Cyclin D1 downregulation. Ironomycin treatment induced DNA damage response, accumulation of DNA  
70 double-strand breaks, and activated the Unfolded Protein Response (UPR). We validated the therapeutic  
71 interest of ironomycin in primary MCL cells of patients. Ironomycin demonstrated a significant higher  
72 toxicity in MCL cells compared to normal cells from the microenvironment. We tested the therapeutic  
73 interest of combining ironomycin with conventional treatments used in MCL. We identified a synergistic  
74 effect when ironomycin is combined with Ibrutinib, Bruton's tyrosine kinase (BTK) inhibitor, associated  
75 with a strong inhibition of B-Cell receptor (BCR) signaling.

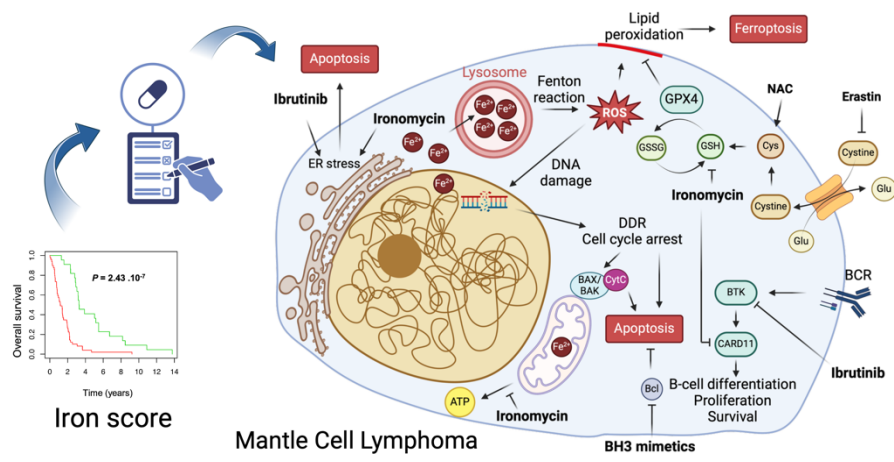
76 Conclusion: Altogether, these data underline that MCL patients may benefit from targeting iron  
77 homeostasis using ironomycin alone or in combination with conventional MCL treatments.

78

79 **Keywords:** Iron metabolism, mantle cell lymphoma, ironomycin, drug combination, B-cell receptor  
80 signaling.

81 Graphical abstract:

82



83

84

85

86

87

88

89

90

91

92

93

94

95

96

97

98

99

100

101

102

103 **Introduction**

104 Mantle cell lymphoma (MCL) is a rare subtype of non-Hodgkin's lymphoma (NHL), that accounts for 5-7%  
105 of all NHL cases. MCL is derived from mostly antigen-naïve cells that proliferate in the mantle zone around  
106 germinal centers. One of the main genetic characteristics of MCL is chromosome translocation t(11;14)  
107 that causes Cyclin D1 overexpression, conferring a proliferative phenotype to tumor cells [1]. In addition,  
108 aberrations of *TP53* in aggressive MCL have a negative impact on survival [2].

109 The median age of MCL patients is 60-70 years [1]. Despite recent advances, it remains incurable and  
110 patients with high-risk disease have particularly poor outcomes. Depending on the age and fitness of the  
111 patient, treatments include conventional chemotherapy and stem cell transplantation (SCT), BTK  
112 inhibitors, or bispecific antibodies against CD19 and CD20, among others. However, drug resistance and  
113 disease progression are major challenges in the treatment of MCL [2].

114 Ibrutinib inhibits BTK, thereby blocking BCR signaling, which is abnormally active in some B-cell cancers,  
115 including lymphomas. Ibrutinib is approved to treat MCL patients that have received at least one previous  
116 line of treatment [3]. In addition, oral BTK inhibitors administered alone [4], or combinations of ibrutinib  
117 with rituximab [5], or ibrutinib with the Bcl2-antagonist venetoclax [6,7], have been proven as interesting  
118 chemotherapy-free targeted therapeutic approaches for MCL patients at relapse [8]. However, primary  
119 and acquired resistance to ibrutinib has already been described in MCL patients [9]. Thus, the study of the  
120 mechanisms of cancer cell resistance to ibrutinib and response to its combination with other drugs is of  
121 great therapeutic interest in treating patients with MCL.

122 Iron is an essential element for cells. It is a critical component of many biological processes such as  
123 mitochondrial function [10], DNA replication and repair [11], and epigenetic modifications [12]. Iron is  
124 also a redox-active metal that can participate in free radical formation and propagation of lipid  
125 peroxidation through the Fenton chemistry reaction, which can cause a type of iron-dependent non-  
126 apoptotic cell death known as ferroptosis [13]. Thus, iron dysregulation is linked to pathological states  
127 [14]. Indeed, cancer cells often present dysregulation of many genes involved in iron metabolism, and  
128 abnormal iron homeostasis is implicated in autoimmunity, tumorigenesis, and the progression of cancers  
129 [15,16]. In the past years, inducing ferroptosis with iron-targeting molecules, such as iron chelators or iron  
130 oxide nanoparticles, has gained attention as a promising anti-cancer strategy in hematologic malignancies  
131 [17–21].

132 Considering the importance of iron homeostasis in cell biology and its implication in cancer, we  
133 investigated the therapeutic potential of targeting the iron pool of MCL cells with ironomycin, a promising  
134 agent known for sequestering iron in lysosomes and inducing cancer cells death [22,23]. Our findings  
135 demonstrate that ironomycin triggers both apoptosis and ferroptosis in MCL cells. Ironomycin also  
136 activates the UPR pathway, a cellular stress response triggered by the accumulation of misfolded or  
137 unfolded proteins in the endoplasmic reticulum (ER). Moreover, we observed a synergistic effect when  
138 ironomycin is combined with ibrutinib, leading to enhanced MCL cell death, suggesting that there is a  
139 therapeutic benefit in the combined approach of BCR inhibition and iron homeostasis targeting for the  
140 treatment of MCL patients.

141

142 **METHODS**

## 143 **Mantle Cell Lymphoma cell lines culture**

144 6 MCL cell lines (JEKO1, JVM2, MAVER1, MINO, REC1, GRANTA519) were purchased from the DSMZ  
145 (Leibniz-Institut DSMZ – GmbH, Germany). They were cultured in RPMI with 10% FBS (JVM2, REC1) or 20%  
146 FBS (JEKO1, MAVER1, MINO); or DMEM with 10% FBS (GRANTA519) at 37 °C and 5% CO<sub>2</sub>. Cells were  
147 passed every 3-4 days.

## 148 **Reagents**

149 Ironomycin (AM5) was a kind gift from Raphaël Rodriguez (patent application WO2016/038223).

150 Deferasirox (ITM101102264, TargetMol), Erastin (S7242, Selleckchem), Ferrostatin-1 (S7243,  
151 Selleckchem), Q-VD Oph (S7311, SelleckChem), Iron (III) Chloride Hexahydrate (31232-M, Sigma Aldrich),  
152 N-Acetyl Cysteine (A9165, Sigma Aldrich), Ibrutinib (S2680, Selleckchem), Venetoclax (S8048, Selleckchem),  
153 AZD-5991 (S8643, Selleckchem), A1155463 (T6748, TargetMol), bendamustine (S5939, Selleckchem),  
154 bortezomib (S1013, Selleckchem).

## 155 **Synergy matrixes**

156 For evaluation of ironomycin synergy with ibrutinib, venetoclax, AZ1159XX and A-1155463 , cells were  
157 seeded at 30000 (JVM2) or 50000 (JEKO1, MAVER1) cells/well and cultured for 4 days in 96-well flat-  
158 bottom plates in the presence of ironomycin (0.01 – 4 µM), ibrutinib (BTK inhibitor; 0.125 -32 µM),  
159 venetoclax (Bcl2 inhibitor; JEKO1/JVM2: 125 – 32000 nM; MAVER1: 0.12 – 8000 nM), AZ1159 (Mcl1  
160 inhibitor; 0.01 – 5 µM), A1155463 (Bcl-xL inhibitor: 0.15 – 40 µM). Increasing concentrations of ironomycin  
161 were combined with increasing concentrations of the other drugs to evaluate all possible combinations.  
162 Cell growth was evaluated using CellTiter-Glo (CTG) Luminiscent Assay (G7573, Promega) according to  
163 manufacturer’s protocol and luminescence was measured using a Centro LB 960 luminometer (Berthold  
164 Technologies). For each combination, the percentage of expected growing cells in the case of effect  
165 independence was calculated with Bliss equation using R package “SynergyFinder”.

166 Supplementary information is included in Supplemental Methods.

## 167 **RESULTS**

### 168 **Iron homeostasis-related gene expression profile identifies high risk MCL patients**

169 According to the major role of iron homeostasis in cancer, we aimed to identify iron metabolism-related  
170 genes associated with a prognostic value in MCL. Sixty-two genes related to iron biology and cancer had  
171 been reported [20,24] (Table S1). Using Maxstat R algorithm [25] and multiple testing correction, we  
172 identified 8 genes with significant prognostic value in a cohort of newly diagnosed MCL patients (n = 71)  
173 [26] (Figure 1A) and combined their prognostic information in a Gene Expression Profile (GEP)-based iron-  
174 score (IS) as previously described [27,28]. IS is defined by the sum of the beta coefficients of the Cox model  
175 for each prognostic gene, weighted by +1 or -1 according to the patient expression signal above or below  
176 the Maxstat value. IS segregated the cohort in two groups (iron-score cut point: -3.7798) with a maximum  
177 difference in overall survival (OS; Figure 1B), underlining that an elevated IS allows the identification of  
178 MCL patients with poor prognosis and dysregulation of iron metabolism who could benefit from targeted  
179 therapy.

### 180 **Targeting iron homeostasis kills MCL cells**

181 We and others reported the therapeutic interest of targeting iron homeostasis with ironomycin to kill  
182 Diffuse Large B-Cell Lymphoma (DLBCL) [20] and Acute Myeloid Leukemia (AML) [29] cells. Using 6 MCL  
183 cell lines, we determined the IC50 of ironomycin. Deferasirox, an iron chelator [30–32] approved by the  
184 FDA to treat chronic iron overload by selectively binding the ferric form of iron [33], was used as control.  
185 Of note, deferasirox was evaluated in MCL cells [19] and reported to have anti-tumoral effects *in vitro*  
186 [34]. Interestingly, IC50 values of ironomycin were in the nanomolar range, whereas those of deferasirox  
187 were in the micromolar range (Figure S1A), indicating that ironomycin is ~100-fold more potent in  
188 inhibiting MCL cells growth. Ironomycin is also significantly toxic to MCL primary cells at nanomolar  
189 concentrations (Figure 1C and Figure S1B). Furthermore, only deferasirox significantly impacted viability  
190 of purified peripheral blood mononucleated cells (PBMC) from healthy donors (Figure 1D). Both  
191 ironomycin and deferasirox were not toxic to normal B- and T-lymphocytes, but killed monocytes in a  
192 dose-dependent manner (Figure 1E). Monocytes are known to participate in iron recycling and  
193 accumulate intracellular iron [35] which makes them more susceptible to drugs targeting iron  
194 homeostasis. Moreover, a small but significant increase in the percentage of T-lymphocytes was also  
195 observed exclusively upon ironomycin treatment.

196 Then, to further characterize the biological effect of ironomycin on MCL cells, we chose 3 cell lines (JEKO1,  
197 JVM2 and MAVER1) with different ironomycin IC50 and that partially represent the molecular  
198 heterogeneity of MCL patients (Table S2). High concentration of deferasirox was used to compare the  
199 effect of iron chelation versus ironomycin-induced iron sequestration. Ironomycin treatment induced a  
200 decrease in proliferation (Figure 2A and Figure S1C) associated with an altered cell cycle distribution  
201 (Figure 2B). In MCL, t(11;14) translocation, which causes the over-expression of the gene *CCND1*, is  
202 associated with high tumor cell proliferation [36]. JVM2 expresses lower protein levels of Cyclin D1 than  
203 other MCL cell lines, while co-expressing Cyclin D2 [37] (Table S2). Importantly, treatment of MCL cells  
204 with ironomycin caused a marked diminution of Cyclin D1 and Cyclin D2 protein levels (Figure 2C,D). We  
205 confirmed that the decrease in Cyclin D1 expression correlated with a decrease in *CCND1* transcription in  
206 JEKO1. However, no difference in mRNA levels of *CCND1/CCND2* were observed in JVM2/MAVER1 (Figure  
207 2E), suggesting that lower protein levels may be due to increased protein degradation. Cyclin D1 is  
208 degraded by the proteasome and it was reported that deferasirox induces proteasome-mediated Cyclin  
209 D1 degradation [19,34]. Indeed, proteasome inhibitor bortezomib rescued Cyclin D1/Cyclin D2  
210 degradation induced by ironomycin and deferasirox (Figure S1D).

211 Furthermore, we analyzed whether ironomycin also impacted the levels of several well-known factors  
212 controlling cell cycle progression and linked to Cyclin D1 (Cdk4, Rb, p53, p21 and p27) [36]. It has been  
213 reported that these MCL cell lines present different abnormalities regarding some of these genes (Table  
214 S2) and we confirmed different protein levels by western blot (Figure 2F). Interestingly, in JEKO1 and  
215 JVM2, ironomycin induced  $\gamma$ H2AX, a marker of DNA double strand breaks and DNA damage response  
216 (DDR) activation [38]. We did not observe  $\gamma$ H2AX in MAVER1, probably due to the inactivation of ATM in  
217 this cell line (Table S2), but Chk2 was slightly phosphorylated in response to ironomycin.

### 218 **Ironomycin causes cell death mediated by apoptosis in MCL cells**

219 Ironomycin significantly reduced cell viability in all cell lines (Figure S1E). Since ironomycin has been  
220 reported to induce ferroptosis, apoptosis and ferritinophagy [20,22,23,29], we sought to identify the  
221 type(s) of cell death that it induces in MCL cells. Ironomycin and deferasirox increased the Annexin V+

222 population (Figure 3A), indicative of apoptotic cell death. Supplementation of cells with FeCl<sub>3</sub> prevented  
223 cell death caused by deferasirox, but not by ironomycin (Figure S2A).

224 Increase in Annexin V+ cells upon ironomycin treatment correlated with caspases 3, 8 and 9 cleavage in  
225 JEKO1 and MAVER1 cell lines, but not in JVM2 (Figure 3B). Given the limited sensitivity of western blot  
226 analysis and the fact that it has been described that caspases 8 and 9 activity is stimulated by dimerization  
227 instead of cleavage [39], we confirmed activation of caspases by the more sensitive CaspaseGlo® Assay.  
228 We observed that ironomycin increased caspase 3 and 8 activity in all three cell lines, although it was only  
229 statistically significant in JEKO1 and JVM2, whereas caspase 9 was only significantly activated in JEKO1  
230 (Figure S2B). Interestingly, pre-treatment of cells with pancaspase inhibitor Quinoline-Val-Asp-  
231 Difluorophenoxymethylketone (Q-VD-Oph) partially rescued cell death in JEKO1 and JVM2 cell lines,  
232 suggesting that apoptosis is not the only cell death type induced by ironomycin in MCL cells (Figure S2C).

233 Cancer cells are frequently addicted to the presence of anti-apoptotic factors, such as the Bcl2 family of  
234 proteins, that are attractive therapeutic targets [40]. We observed significant changes in the levels of Bcl  
235 family anti- and pro-apoptotic factors upon ironomycin treatment that were cell line dependent. In JEKO1  
236 cells, ironomycin induced the degradation of all factors, whereas it caused an increase in JVM2 and  
237 MAVER1 (Figure 3C). Given these differences, we used the complementary *in vitro* assay BH3 profiling [41]  
238 to measure the apoptotic priming of cells and their dependences on the anti-apoptotic proteins Bcl2, Bcl-  
239 xL and Mcl1 upon drug treatment (Figure S3A). We observed an increased dependence on these proteins  
240 in JEKO1, and specially to Bcl2 in JVM2/MAVER1 (Figure 3D). Moreover, combining ironomycin with Bcl2i,  
241 Bcl-xLi and Mcl1i, resulted in synergistic effects across all cell lines, confirming that ironomycin sensitizes  
242 MCL cells to Bcl2-family inhibitors (Figure S3B-D) that have been evaluated in relapsed MCL patients with  
243 promising results [42,43].

244 In response to ironomycin, Cytochrome C level was decreased in JEKO1, and increased in JVM2/MAVER1  
245 (Figure S4A). It was reported that up-regulation of Cytochrome C is linked to caspase activation and  
246 triggering of cell death [44]. In addition, severe mitochondria damage is associated with higher  
247 Cytochrome C release into the extracellular space and higher cell death levels [45]. Therefore, the  
248 different levels of Cytochrome C in the cell lines may be explained by their different sensitivity to  
249 ironomycin. Thus, it is possible that Cytochrome C increase in JVM2 and MAVER1 is linked to moderate  
250 apoptosis level and its decrease in JEKO1 may be due to higher levels of cell death (Figure 3A) and loss of  
251 cell membrane integrity, which will release cytosolic proteins like Cytochrome C to the medium, that will  
252 then be less abundant by western blot. To test this hypothesis, we removed JEKO1 dead cells by Ficoll®  
253 centrifugation and performed western blot only on living cells with unbroken cell membrane. The levels  
254 of Cytochrome C did not decrease in these cells in ironomycin vs untreated conditions (Figure S4A). In  
255 contrast to our previous result (Figure 3C), after dead cell removal, the only anti-apoptotic factor that was  
256 actually decreased by ironomycin in JEKO1 cells was Mcl1, whereas the pro-apoptotic proteins Bax and  
257 Bak remained unchanged (Figure S4B). In basal conditions, Cytochrome C is necessary for ATP production  
258 in the mitochondria and needs iron. We treated cells with increasing doses of ironomycin for 48 h and  
259 used CellTiter Glo assay to quantify intracellular ATP. Our results showed a significant dose-dependent  
260 decrease in the levels of ATP (Figure S4C), most likely due to iron depletion caused by ironomycin. Using  
261 Seahorse functional assay, we confirmed that ironomycin strongly decreased both basal and maximal  
262 mitochondrial respiration capacities (Figure S4D). These data indicate that ironomycin impairs  
263 mitochondrial function, eventually triggering caspase-dependent apoptosis.



## 264 Ironomycin induces ferroptosis in MCL cells

265 Ferrostatin-1 [46], a ferroptosis inhibitor, rescued ironomycin- and erastin-induced cell death (Figure 3E),  
266 confirming that ironomycin also induces ferroptosis in MCL cells. Erastin was used as a positive control  
267 [47]. Finally, we studied if ironomycin activated autophagy in MCL cells. BIX1294 was used as a positive  
268 control [48]. No formation of LC3B foci [49], was observed upon ironomycin treatment (Figure S4E).  
269 However, western blot analysis showed a modest increase in LC3B-II in JVM2, and a degradation (JEKO1  
270 and MAVER1) or accumulation (JVM2) of ferritin, an iron-storage protein which is degraded when  
271 ferritinophagy is activated [50] (Figure S4F-H). Since ferritinophagy triggers ferroptosis and our western  
272 blot analysis showed differences in Ferritin and LC3B levels between the three cell lines (Figure S4G), we  
273 cannot exclude that ferritinophagy also contributes to ferroptosis initiation in MCL cells. Interestingly,  
274 increased expression of *TFRC*, which codes for the transferrin receptor CD71 and has a prognostic value  
275 according to our analysis (Figure 1A,B), is associated with more aggressive forms and poor prognosis in  
276 MCL [51]. We confirmed higher levels of CD71 in MCL cell lines and primary MCL cells from patients than  
277 in PBMC from healthy donors (Figure S4H). Furthermore, upon treatment with ironomycin, we observed  
278 an increase in CD71 protein levels, a marker of ferroptosis (Figure S4I). Finally, we pretreated cells with  
279 Q-VD-Oph, ferrostatin-1 or combination of both (Figure S4J), and confirmed that ironomycin triggers both  
280 apoptosis and ferroptosis in MCL cells.

281 Ironomycin has been involved in the generation of ROS, that cause lipid peroxidation and DNA damage  
282 [20] (Figure S4F). In agreement, we observed a small but significant increase in ROS production induced  
283 by ironomycin that could not be rescued by iron supplementation (Figure S5A). Intriguingly, combination  
284 of exogenous iron and ironomycin led to increased ROS production in JEKO1 and JVM2 compared to  
285 ironomycin alone, while it reverted ROS production in combination with deferasirox in JVM2 and MAVER1.  
286 Of note, JEKO1 showed an elevated level of ROS already in basal conditions (Figure S5B), that correlated  
287 with  $\gamma$ H2AX indicative of DNA damage (Figure 2F). This elevated basal ROS level may contribute to the  
288 stronger sensitivity of JEKO1 to ironomycin treatment compared to JVM2, in which a 5 times higher  
289 concentration of ironomycin was required to reach similar levels of  $\gamma$ H2AX (Figure 2F). Given the central  
290 role of iron in mitochondria, we also analyzed the production of mitochondrial ROS using the specific  
291 probe MitoSox. No significant increase of mitochondrial ROS was detected upon ironomycin or deferasirox  
292 treatment (Figure S5C). Given that ROS cause lipid peroxidation that in turn triggers ferroptosis, we used  
293 BODIPY dye to monitor lipids oxidation state. BODIPY underlined a significant increase in peroxidized lipids  
294 upon ironomycin and erastin treatments, that was diminished by ferrostatin-1 (Figure S5D). The  
295 phospholipid hydroperoxidase GPX4 protects cells against membrane lipid peroxidation and is involved in  
296 ferroptosis regulation [50]. Intriguingly, GPX4 levels varied differently in each MCL cell line in response to  
297 ironomycin (Figure S4A,B).

298 Vitamin E is an antioxidant that has been reported to prevent ferroptosis [52]. High-density lipoproteins  
299 (HDL) and low-density lipoproteins (LDL) can carry Vitamin E to cells to mitigate lipid peroxidation and  
300 ferroptosis [53]. In order to evaluate the contribution of lipids to the cellular effects of ironomycin, we  
301 cultured cells in medium supplemented with lipid-free serum. Lack of exogenous lipids induced cell death  
302 in untreated JVM2 and MAVER1 cell lines, with no effect on JEKO1, suggesting that the three cell lines are  
303 metabolically different in basal conditions (Figure S6A). Treatment with ironomycin in absence of lipids  
304 only increased cell death in JVM2 cells. ROS production was diminished in JEKO1 and MAVER1 in lipid-  
305 depleted medium, but not in JVM2 (Figure S6B). Lipid peroxidation was increased in absence of lipids in  
306 all cell lines, and treatment with ironomycin led to a small but significant increase in JEKO1 and JVM2



307 (Figure S6C). Scavenger Receptor Class B Type I (SR-B1) is an HDL receptor that facilitates cholesterol  
308 esters uptake and the bi-directional flux of free cholesterol. SR-B1 has been reported as a mediator of  
309 oxidative events in cancer [54]. Western blot analysis showed that the three MCL cell lines presented  
310 different levels of expression of SR-B1 that were not changed by ironomycin (Figure S6D). We monitored  
311 the presence of lipid droplets, the organelles that store triacylglycerols and sterol esters, using the Nile  
312 Red dye, which marks polar and neutral lipids including cholesterol esters [55]. Surprisingly, no lipid  
313 droplets were observed in JVM2, whereas ironomycin decreased lipid droplets in both JEKO1 and MAVER1  
314 (Figure S6E).

315 We have shown that iron supplementation was not able to rescue ironomycin-induced cell death (Figure  
316 S2A), but we investigated if any of the cellular responses induced by ironomycin treatment could be  
317 reversed by iron supplementation. As before, deferasirox was used as a control. Addition of iron rescued  
318 the degradation of Cyclin D1, ATF6, Bcl-xL and Mcl1 caused by deferasirox, as well as the increase in  $\gamma$ H2AX  
319 in the three cell lines. However, no consistent changes in protein abundance were detected upon iron  
320 supplementation in ironomycin-treated cells, with JVM2 being the only cell line in which the accumulation  
321 of Bcl-xL, Bcl2, GPX4 and Cytochrome C was reverted by  $\text{FeCl}_3$  addition (Figure S7). The numerous cellular  
322 effects of ironomycin in the three MCL cell lines studied are summarized in Table S3.

323

#### 324 **Ironomycin induces dysregulation of BCR pathway**

325 In order to better understand the global effect of targeting iron homeostasis in MCL, we performed RNA-  
326 sequencing (RNA-seq) analysis of MCL cell lines treated with ironomycin. Among the 174 genes  
327 significantly differentially expressed, Gene Set Enrichment Analysis (GSEA) analysis showed that UPR was  
328 the most upregulated pathway by ironomycin treatment, whereas innate immune system pathways were  
329 the most downregulated (Figure 4A). We confirmed that ironomycin induced the accumulation or  
330 phosphorylation of several UPR proteins, including IRE1 $\alpha$  as well as the generation of XBP1s, indicative of  
331 UPR signaling activation (Figure 4B).

332 Regarding downregulated pathways identified by RNA-seq (Figure 4A), we hypothesized that  
333 downregulation of BCR-related genes induced by ironomycin could potentiate the cytotoxic effect of BCR-  
334 inhibiting therapy in MCL. Aberrant BCR activation is a key pro-survival pathway that includes BTK, NF- $\kappa$ B  
335 and AKT. Ibrutinib is an inhibitor of BTK used in the treatment of MCL. However, drug resistance frequently  
336 leads to patient relapse [56]. JEKO1 and JVM2 are ibrutinib-sensitive or mild-sensitive cell lines, whereas  
337 MAVER1 is resistant (Figure S8A). Using synergy matrixes, we found that ironomycin and ibrutinib  
338 synergize to inhibit MCL cells growth (Figure 4C-E). Interestingly, ironomycin combined with ibrutinib  
339 induced a downregulation of genes involved in the BCR signaling pathway including *CARD11*, *CD22*, *PTPN6*,  
340 *IGLV1-47* and *IGLV1-44* (Figure S8B) [56]. We confirmed *CARD11* downregulation by western blot (Figure  
341 S8C). These results highlight the therapeutic potential of combining ironomycin and ibrutinib to enhance  
342 the cytotoxic effects of BTK inhibition, even in ibrutinib-resistant MCL cells.

343 In order to understand the molecular mechanism of this synergy, we studied if ironomycin could regulate  
344 the activation of the BCR pathway. In basal conditions, MCL cell lines presented different activation level  
345 of BCR downstream pathways. Drug combination inhibited NF- $\kappa$ B in JEKO1, and BTK and Akt in JVM2. In  
346 MAVER1 cell line, the only significant ironomycin effect was the decrease of *CARD11* (Figure S8C-E).

347 Furthermore, we observed that the combination of both drugs significantly reduced cell proliferation and  
348 induced cell cycle arrest to a greater extent than either drug alone (Figure 5A,B). It also induced strong  
349 Cyclin D1 degradation in JEKO1 and moderate in JVM2, together with DNA damage induction (Figure  
350 9A,B). The decrease in proliferation caused by the drug combination correlated with an increase in  
351 Annexin V+ cells (Figure 5C). Caspases and PARP cleavage were observed in JEKO1 and MAVER1 (Figure  
352 S9C). Moreover, Mcl1 was specifically degraded upon drug combination in JEKO1 cell line, whereas Bcl2  
353 seemed to slightly accumulate in JVM2 (Figure S9D). In order to better understand the molecular  
354 mechanism of the synergy, we compared RNA-seq data of cells treated with ironomycin, ibrutinib and the  
355 combination of both drugs. At the studied doses, ibrutinib impacted the expression of a low number of  
356 genes (22 downregulated and 4 upregulated), but no particular pathway was identified (Table S4).  
357 Ironomycin-induced up-regulation of UPR and mTORC signatures was stronger in combination with  
358 ibrutinib specially in JEKO1 and MAVER1 (Figure 5D). Taken together, these results indicate that  
359 combination of ironomycin with ibrutinib induces a sustained activation of UPR and a strong inhibition of  
360 BCR signaling that trigger toxicity in MCL cells.

## 361 Discussion

362 Here, we show that targeting iron homeostasis could be of therapeutic interest to target MCL cells, in  
363 particular in combination with BTK inhibition. First, using MCL patient data, we identified that  
364 deregulation of the expression of iron homeostasis genes can delineate MCL patients with poor outcome  
365 (Figure 1A). High expression of genes coding for transferrin receptor (*TFRC*), transcription factor *HIF1-A*  
366 (hypoxia induced factor 1A), *APEX1* (APEX endonuclease) and *SLC39A14* was associated to a poor  
367 outcome, whereas upregulation of *IREB2* (iron-responsive element binding protein 2), *SCARA3*, *SFXN4*  
368 (sideroflexin-4) and *ABCG2* correlated to a good prognosis. These genes were previously reported to be  
369 involved in other malignancies, but this is the first study that links six of them to MCL. *TFRC* and *HIFs* are  
370 upregulated in many types of cancer, which correlates with poor prognosis and response to therapy  
371 [57,58]. In particular, elevated *HIF1A* was related to poor prognosis in MCL [59]. APEX is activated in  
372 response to DNA damage and its dysregulation is associated to several types of cancer [60]. *SLC39A14*  
373 codes for a metal transporter and was reported downregulated in prostate cancer [61] and upregulated  
374 in glioma [62]. *IREB2* stabilizes the mRNA of *TFRC* and *DMT1* that code for iron transporters, leading to  
375 increased intracellular iron concentration [63] and is dysregulated in lung [64] and renal cancers [65].  
376 Downregulation of ROS scavenger *SCARA3* was reported in prostate cancer [66], hepatocellular carcinoma  
377 [67], lung cancer [68,p.3] and myeloma [69]. Sideroflexin-4 has been suggested as a therapeutic target in  
378 ovarian cancer [70]. Thus, iron dysregulation is an important feature in cancer biology with various effects  
379 depending on the cancer cell type.

380 The iron chelators deferasirox and deferoxamine are approved by the FDA for treatment of chronic iron  
381 overload in patients who are receiving long-term blood transfusions and for conditions such as beta-  
382 thalassemia and other chronic anemias [33,71]. Regarding their use in cancer treatment, previous pre-  
383 clinical studies reported that iron chelation may be of therapeutic interest to treat AML in combination  
384 with vitamin D3 [72] and triggers the DNA damage response in T-cell acute lymphoblastic leukemia [73].  
385 It was reported that deferasirox and vitamin D synergize to promote monocyte differentiation in primary  
386 AML cells and prolonged the survival of AML patients [74]. Moreover, deferasirox is cytotoxic to  
387 lymphoma cells [75], lung cancer cells [76], and multiple myeloma cells [77] among others, and synergizes  
388 with gemcitabine to inhibit pancreatic cancer cell growth [78]. In addition, other pre-clinical studies using  
389 cell lines suggested that deferoxamine or deferasirox may be interesting for MCL treatment [19,34], but

390 none of these agents has been approved for cancer treatment. From a safety point of view, it was reported  
391 that treatment with deferasirox presents a risk of kidney failure [79], liver failure [80,81] and  
392 gastrointestinal bleeding [82] in some patients. Ironomycin, a synthetic derivate of salinomycin that  
393 sequesters iron in the lysosomes and triggers ferroptosis [22,p.5], has demonstrated greater efficacy in  
394 killing various types of cancer cells compared to iron chelators [20,29], owing to its iron-sequestration  
395 specific mechanism of action. In fact, it was described that ironomycin can alter the redox state within  
396 lysosomes, increasing ROS production, and induces lysosomal membrane permeabilization, leading to the  
397 release of potentially toxic lysosomal enzymes and ROS into the cytosol that can further damage  
398 lysosomes and other cellular structures [22].

399 Our results show that ironomycin is toxic to MCL cells at ~100-fold lower concentrations than deferasirox,  
400 suggesting that its side effects if used in cancer therapy would be less than those of deferasirox. In this  
401 regard, our previous study using mouse models showed that mice weight was not affected by ironomycin  
402 treatment at doses that presented toxicity against DLBCL xenografts [20]. Moreover, we found that  
403 ironomycin and deferasirox affect primary MCL cells from patients and normal monocytes without  
404 inducing toxicity in normal B- and T-lymphocytes (Figure 1). Intriguingly, we observed a small but  
405 significant increase in T-lymphocyte percentage upon ironomycin treatment. Given that these cells do not  
406 proliferate in our *in vitro* conditions and that iron homeostasis is important for T-lymphocytes [83], we  
407 surmise that dead monocytes may release iron to the medium that may be up taken by the T-lymphocytes  
408 in the culture, improving their survival compared to control conditions. Since we only evaluated the global  
409 CD3+ T-cell population, further analyses are required to determine which T-lymphocyte sub-population is  
410 more abundant and its intracellular iron level upon ironomycin treatment and its impact in *in vivo* models.  
411 Using MCL cell lines, we studied the molecular mechanisms of ironomycin cytotoxicity. Chromosome  
412 translocation t(11;14) is a genetic hallmark of MCL patients that results in overexpression of Cyclin D1,  
413 which is essential to the pathogenesis of this disease by conferring a proliferative advantage to tumor  
414 cells [1]. In fact, high-risk MCL is associated to proliferation marker Ki-67  $\geq 30\%$  [84,85]. Importantly, we  
415 found that ironomycin induces degradation of Cyclin D1 protein, which correlates with a strong decrease  
416 in cell proliferation and cell cycle arrest (Figure 2). Our data indicate that Cyclin D1 and D2 down-  
417 regulation is due to changes in transcription and increased protein degradation. On the one hand,  
418 epigenetic enzymes such as the Jumonji family of histone demethylases or the DNA Ten-Eleven  
419 Translocation (TET) methylcytosine dioxygenases have been reported to depend on iron as a co-factor  
420 [12]. Thus, iron depletion caused by ironomycin would have an impact on epigenetic and transcriptional  
421 regulation through these enzymes. Moreover, our results show that ironomycin activates an UPR  
422 characterized by the accumulation of IRE1 $\alpha$  (Figure 4B). IRE1 $\alpha$  is responsible for the regulated IRE1 $\alpha$ -  
423 dependent decay (RIDD) that cleaves selected mRNAs, decreasing the proteins that they code for [86].  
424 Thus, it is possible that constitutive UPR activation and IRE1 $\alpha$  accumulation lead to degradation of mRNA  
425 coding for Cyclin D1. On the other hand, UPR activation characterized by p-eIF2 $\alpha$  like in JVM2 and  
426 MAVER1 (Figure 4B) induced by ironomycin can also lead to translation attenuation, which will eventually  
427 reduce Cyclin D1 and Cyclin D2 levels due to protein turnover coupled to lack of new protein synthesis.  
428 Mutation or deletion of *TP53*, which is a major cell cycle regulator, is related to high-risk disease [87,88].  
429 Interestingly, our data show that ironomycin triggers apoptosis in the three MCL cell lines independently  
430 of their *TP53* status (Table S2). These findings strengthen the potential of targeting iron homeostasis as a  
431 way to impair MCL cells growth and slow down tumor progression, even in *TP53* dysregulated patients.

432 We observed that ironomycin induced changes in the abundance of pro-apoptotic and anti-apoptotic  
433 proteins of the Bcl-family. In JEKO1, the anti-apoptotic protein Mcl1 was the main factor degraded, which  
434 explains the triggering of apoptosis. In JVM2/MAVER1 upon ironomycin treatment, all studied factors  
435 accumulated independently of if they were pro- or anti-apoptotic. It was published that Bak interacts with  
436 Mcl1 and that disrupting this interaction induces Mcl1 degradation [89]. Bax expression is regulated by  
437 the tumor suppressor p53 and has been shown to be involved in p53-mediated apoptosis. The association  
438 and the ratio of Bax to Bcl2 also determines survival or death of a cell following an apoptotic stimulus. In  
439 JVM2, which expresses wild type p53, we observed a significant increase in Bax, Bcl-xL, Bcl2 and Mcl1  
440 levels. Our BH3-profiling data show that JVM2 is mostly dependent on Bcl2, with lower dependence on  
441 Mcl1 or Bcl-xL. In MAVER1, Bax and Bcl2 expression inversely correlated, maybe due to a lack of functional  
442 p53 in this cell line. Our BH3-profiling assay confirmed a greater dependence of MAVER1 on Bcl-2,  
443 suggesting that the slight increase in Bax observed by western blot is not sufficient to efficiently trigger  
444 caspase-dependent apoptosis as observed in our other data (Figure S2). In addition, upon DNA damage  
445 caused by ROS, anti-apoptotic proteins like Bcl2 and Bcl-xL can be upregulated or activated in an attempt  
446 to delay or prevent apoptosis, allowing the cell to repair the damage. If the damage is irreparable, the  
447 pro-apoptotic signals may override the anti-apoptotic mechanisms, leading to cell death.

448 In addition, ironomycin induced ROS production, lipid peroxidation, DNA damage and sustained UPR  
449 activation, leading to apoptosis and ferroptosis. Of note, these effects were achieved using nanomolar  
450 concentrations of ironomycin, in contrast to deferasirox which exhibited cytotoxicity at concentrations  
451 10-100 times higher, suggesting that ironomycin could be used at low dose to minimize toxicity and side  
452 effects. The toxicity of ironomycin was already investigated in mice and did not underline significant  
453 toxicities in the range of doses deleterious for cancer cells [20,22,29]. Moreover, iron supplementation  
454 was able to rescue cell death caused by deferasirox, but not by ironomycin, indicating that the cytotoxicity  
455 of ironomycin is not due to limited iron availability for metabolic and enzymatic reactions and therefore  
456 its therapeutic potential diverges from that of iron chelators. We previously reported the efficacy of  
457 ironomycin in targeting B-lymphoma cells using a syngeneic A20 murine model [20]. Further investigation  
458 using specific PDX models is needed to determine optimal ironomycin doses to kill MCL cells and to assess  
459 toxicity *in vivo*.

460 Ironomycin was described to induce ferroptosis by causing lipid peroxidation. We analyzed the  
461 contribution of lipids to ironomycin cytotoxicity and found that lipid deprivation in culture medium had  
462 different effects depending on the cell line (Figure S6). Lack of exogenous lipids only increased the toxicity  
463 of ironomycin in JVM2 cells (Figure S6A) which does not present TAG and sterol esters accumulated in  
464 lipid droplets. This result suggests that the capacity of JVM2 to cope with lipid peroxidation is mostly  
465 dependent on its ability to uptake lipids from the medium to substitute the oxidized ones, since its  
466 intracellular lipid stock is low. The cytotoxicity of ironomycin on JEKO1 and MAVER1 was not affected by  
467 the lack of exogenous lipid source. Both cell lines present lipids stored in lipid droplets, which number and  
468 size was decreased upon ironomycin treatment (Figure S6E), probably due to the use of those stored lipids  
469 to try and repair the ROS-damaged membranes. These results point at the importance of lipids as targets  
470 of ironomycin toxicity and raise the question of how lipid metabolism could impact the response to drugs  
471 targeting iron homeostasis. It has already been reported that lipid metabolism modulates the DNA  
472 damage response [90], which can impact cell response to chemotherapy. Since pharmacological and  
473 dietary manipulations of lipids are possible, it would be interesting to assess a potential synergy between  
474 decreasing the pool of lipids and targeting iron homeostasis as a therapeutic strategy to kill cancer cells.

475 It has been described that sustained ER-stress causes the UPR to trigger apoptosis [91]. Interestingly, we  
476 found that ironomycin upregulates the UPR, notably related to IRE1 $\alpha$  accumulation and activation. The  
477 proteasome inhibitor bortezomib, currently under clinical investigation in MCL, similarly activates an  
478 apoptotic UPR in multiple myeloma [92], suggesting that targeting iron in combination with proteasome  
479 inhibitors may hold therapeutic promise. IRE1 $\alpha$  has kinase and RNase activities [93] and produces the  
480 spliced form XBP1s that targets genes coding for proteins that enhance protein folding capacity and  
481 quality control [94]. High activation of IRE1 $\alpha$  can also cleave other mRNAs with similar structure to that of  
482 XBP1, causing apoptosis [86]. IRE1 $\alpha$  activates the apoptotic signaling kinase 1 (ASK1), which in turn triggers  
483 downstream factors such as JNK and p38 MAPK, enhancing apoptosis. In addition, it has been shown that  
484 persistent ER stress produces ROS [95]. These notions raise the idea that ironomycin induced-ROS  
485 production leading to ER stress and UPR activation that will in turn produce more ROS, creating an  
486 amplification loop culminating in apoptosis. Moreover, there is increasing evidence of a link between UPR,  
487 in particular IRE1 $\alpha$ , and lipid metabolism regulation [96]. Ironomycin caused lipid peroxidation, which  
488 must be replaced by new lipids to maintain membrane integrity. ER regulates lipid synthesis and is itself  
489 tightly regulated by UPR [97], which may explain UPR activation and IRE1 $\alpha$  accumulation upon  
490 ironomycin-dependent lipid peroxidation. Interestingly, it has also been reported that IRE1 $\alpha$  can trigger  
491 mitochondrial (intrinsic) apoptosis in a Bax/Bak-dependent manner [91] and ironomycin triggers a non-  
492 canonical Bax/Bak-dependent apoptosis in AML [29]. Our BH3 profiling experiments show that ironomycin  
493 changes the dependencies of MCL cells to Bcl2-family anti-apoptotic factors and induces changes in BAX  
494 expression (Figure 3C,D and Figure S3). We found a synergy between iron dysregulation and inhibitors of  
495 Bcl2-family anti-apoptotic factors which could be of therapeutic interest. Moreover, we proved that  
496 ironomycin caused significant changes in basal and maximal mitochondrial respiratory capacities and  
497 reduced ATP production (Figure S4C,D). Altogether, these results indicate that ironomycin exerts  
498 profound toxicity on mitochondria, triggering apoptosis in MCL cells, as well as ferroptosis linked to ROS  
499 production and lipid peroxidation. Unlike in DLBCL cells [20], ironomycin seemed to not cause  
500 ferritinophagy in all MCL cell lines, suggesting that malignant B-cells from diverse origins exhibits distinct  
501 vulnerabilities related to iron metabolism.

502 MCL is characterized by aberrant activation of the BCR pathway, which is initiated by BCR stimulation and  
503 BTK activation to regulate the downstream NF- $\kappa$ B and PI3K/AKT/mTOR pathways. Thus, BTK inhibitors  
504 such as ibrutinib are used in relapse/refractory MCL patients with good initial response [98] and the  
505 benefit of BTK inhibitors use earlier in the treatment course is under investigation with encouraging  
506 results [8,99–102]. However, resistance to ibrutinib is very frequent and new strategies to overcome it  
507 using drug combination are being explored [8,99–102] (ENRICH clinical trial: ISRCTN11038174). It has been  
508 suggested that B-cells resistance to ibrutinib can have different origins including gene mutation,  
509 transcriptional dysregulation or tumor microenvironment mediation [103]. Through RNA-seq, we found  
510 that ironomycin downregulates a BCR signature and confirmed the reduction of CARD11 protein, a BCR  
511 pathway downstream factor. CARD11 gain-of-function was also shown to induce BCL2A1 expression and  
512 promote drug resistance in MCL [104]. This prompted us to investigate the combination of ironomycin  
513 with ibrutinib, which synergized to kill MCL cells even in ibrutinib-resistant MAVER1 cell line. Our data  
514 indicate that ironomycin and ibrutinib synergize to impair MCL cells proliferation and cause sustained  
515 elevated UPR activation incompatible with cell survival. Moreover, combination of venetoclax and  
516 ibrutinib to treat relapse/refractory MCL patients showed a remission rate of 71% [6]; however, resistance  
517 to this drug combination has been reported [105]. Currently, an ongoing phase 3 clinical trial (SYMPATICO:  
518 #NCT03112174) is evaluating the combination ibrutinib plus venetoclax vs ibrutinib alone in relapsed MCL



519 patients. We observed a synergy of ironomycin with both venetoclax and ibrutinib (Figure S3), suggesting  
520 that targeting iron homeostasis could be a promising strategy for patients who develop drug resistance.  
521 The mechanisms of ironomycin effect alone and in combination with other drugs analyzed in this study,  
522 namely ibrutinib and Bcl2-family inhibitors, are summarized in the model in Figure 6. Altogether, our  
523 findings underscore the therapeutic potential of targeting iron homeostasis to overcome drug resistance  
524 in MCL.

525

## 526 **Acknowledgements**

527 We acknowledge the imaging facility MRI, member of the France-BioImaging national infrastructure  
528 supported by the French National Research Agency (ANR-10-INBS-04, “Investments for the future”). The  
529 J. Moreaux research group was supported by grants from INCA PLBIO22 PIC-ASO (INCA\_16734), ANR-23-  
530 CE15-0016-01 EPI-B-PLASMADIFF, SIRIC Montpellier Cancer (INCa-DGOS-INSERM- ITMO Cancer\_ 18004),  
531 ARC foundation PGA EpiMM3D, Institut Carnot CALYM and a grant CALYM-Janssen, FFRMG (AAP-FFRMG-  
532 2021), AAP ECOPHYTO – PELYCANO (This action is led by the Ministries for Agriculture and Food  
533 Sovereignty, for an Ecological Transition and Technical Cohesion, for Health and Prevention, and for  
534 Higher Education and Research, with the financial support of the French Office for Biodiversity, as part of  
535 the call for projects on the Ecophyto II+ plan "Pgytosanitary products : from exposure to impacts on human  
536 health and ecosystems towards an integrated "one health" approach", with the fees for diffuse pollution  
537 coming from the Ecophyto II+ plan), AAP READYNOV, MSDAVENIR EpiMuM-3D, Institut Universitaire de  
538 France and by the European Union (Project 101097094 — ELMUMY. Views and opinions expressed are  
539 however those of the author(s) only and do not necessarily reflect those of the European Union or HADEA.  
540 Neither the European Union nor the granting authority can be held responsible for them). Views and  
541 opinions expressed are however those of the author(s) only and do not necessarily reflect those of the  
542 European Union or HADEA. Neither the European Union nor the granting authority can be held responsible  
543 for them. SO is supported by a grant from Fondation de France. JER is supported by la Ligue Nationale  
544 Contre le Cancer “Équipe Labellisée” and l’Agence Nationale de la Recherche (LABEX SIGNALIFE ANR-11-  
545 LABX-0028-01).

546

## 547 **Authorship Contributions, Conflict of Interest Disclosures**

548 SO: designed and performed the research, analyzed the data and wrote the paper. LA and JD: performed  
549 the research, analyzed the data and participated in the writing of the paper. HdB, MA, EGP, OK, GR, NR:  
550 participated in the research. MLZ performed bioinformatic analyses. VJ, AR and SA: performed the BH3  
551 profiling experiments. TC, GC, CH, JC, JER, RR: participated in the research and in the writing of the paper.  
552 CB and JM: acquired the funding, supervised the research and the writing of the paper.

## 553 **Conflict of Interest Disclosures**

554 The authors declare no conflict of interest.

## 555 **REFERENCES**

556 [1] Armitage JO, Longo DL. Mantle-Cell Lymphoma. N Engl J Med. 2022; 386(26): 2495–2506.

- 557 [2] Jain P, Wang ML. Mantle cell lymphoma in 2022—A comprehensive update on molecular  
558 pathogenesis, risk stratification, clinical approach, and current and novel treatments. *American J*  
559 *Hematol.* 2022; 97(5): 638–656.
- 560 [3] de Claro RA, McGinn KM, Verdun N, et al. FDA Approval: Ibrutinib for Patients with Previously  
561 Treated Mantle Cell Lymphoma and Previously Treated Chronic Lymphocytic Leukemia. *Clinical*  
562 *Cancer Research.* 2015; 21(16): 3586–3590.
- 563 [4] Wang M, Shah NN, Alencar AJ, et al. LOXO-305, A Next Generation, Highly Selective, Non-Covalent  
564 BTK Inhibitor in Previously Treated Mantle Cell Lymphoma, Waldenström’s Macroglobulinemia,  
565 and Other Non-Hodgkin Lymphomas: Results from the Phase 1/2 BRUIN Study. *Blood.* 2020;  
566 136(Supplement 1): 8–10.
- 567 [5] Jain P, Romaguera J, Srouf SA, et al. Four-year follow-up of a single arm, phase II clinical trial of  
568 ibrutinib with rituximab (IR) in patients with relapsed/refractory mantle cell lymphoma (MCL). *Br*  
569 *J Haematol.* 2018; 182(3): 404–411.
- 570 [6] Tam CS, Anderson MA, Pott C, et al. Ibrutinib plus Venetoclax for the Treatment of Mantle-Cell  
571 Lymphoma. *N Engl J Med.* 2018; 378(13): 1211–1223.
- 572 [7] Zhao S, Kanagal-Shamanna R, Navsaria L, et al. Efficacy of venetoclax in high risk relapsed mantle  
573 cell lymphoma ( MCL ) - outcomes and mutation profile from venetoclax resistant MCL patients.  
574 *Am J Hematol.* 2020; 95(6): 623–629.
- 575 [8] Jain P, Zhao S, Lee HJ, et al. Ibrutinib With Rituximab in First-Line Treatment of Older Patients  
576 With Mantle Cell Lymphoma. *JCO.* 2022; 40(2): 202–212.
- 577 [9] Hershkovitz-Rokah O, Pulver D, Lenz G, et al. Ibrutinib resistance in mantle cell lymphoma: clinical,  
578 molecular and treatment aspects. *Br J Haematol.* 2018; 181(3): 306–319.
- 579 [10] Paul BT, Manz DH, Torti FM, et al. Mitochondria and Iron: current questions. *Expert Rev Hematol.*  
580 2017; 10(1): 65–79.
- 581 [11] Zhang C. Essential functions of iron-requiring proteins in DNA replication, repair and cell cycle  
582 control. *Protein Cell.* 2014; 5(10): 750–760.
- 583 [12] Farida B, Ibrahim KG, Abubakar B, et al. Iron deficiency and its epigenetic effects on iron  
584 homeostasis. *J Trace Elem Med Biol.* 2023; 78: 127203.
- 585 [13] Dixon SJ, Lemberg KM, Lamprecht MR, et al. Ferroptosis: An Iron-Dependent Form of  
586 Nonapoptotic Cell Death. *Cell.* 2012; 149(5): 1060–1072.
- 587 [14] Battaglia AM, Chirillo R, Aversa I, et al. Ferroptosis and Cancer: Mitochondria Meet the “Iron  
588 Maiden” Cell Death. *Cells.* 2020; 9(6): 1505.
- 589 [15] Hassannia B, Vandenabeele P, Vanden Berghe T. Targeting Ferroptosis to Iron Out Cancer. *Cancer*  
590 *Cell.* 2019; 35(6): 830–849.



- 591 [16] Morales M, Xue X. Targeting iron metabolism in cancer therapy. *Theranostics*. 2021; 11(17):  
592 8412–8429.
- 593 [17] Li J, Zhang W. From iron chelation to overload as a therapeutic strategy to induce ferroptosis in  
594 hematologic malignancies. *Hematology*. 2022; 27(1): 1163–1170.
- 595 [18] Wang Y, Yu L, Ding J, et al. Iron Metabolism in Cancer. *IJMS*. 2018; 20(1): 95.
- 596 [19] Vazana-Barad L, Granot G, Mor-Tzuntz R, et al. Mechanism of the antitumoral activity of  
597 deferasirox, an iron chelation agent, on mantle cell lymphoma. *Leukemia & Lymphoma*. 2013;  
598 54(4): 851–859.
- 599 [20] Devin J, Cañeque T, Lin Y-L, et al. Targeting Cellular Iron Homeostasis with Ironomycin in Diffuse  
600 Large B-cell Lymphoma. *Cancer Research*. 2022; 82(6): 998–1012.
- 601 [21] Pullarkat V, Meng Z, Donohue C, et al. Iron chelators induce autophagic cell death in multiple  
602 myeloma cells. *Leukemia Research*. 2014; 38(8): 988–996.
- 603 [22] Mai TT, Hamai A, Hienzsch A, et al. Salinomycin kills cancer stem cells by sequestering iron in  
604 lysosomes. *Nature Chem*. 2017; 9(10): 1025–1033.
- 605 [23] Versini A, Colombeau L, Hienzsch A, et al. Salinomycin Derivatives Kill Breast Cancer Stem Cells by  
606 Lysosomal Iron Targeting. *Chem Eur J*. 2020; 26(33): 7416–7424.
- 607 [24] Miller LD, Coffman LG, Chou JW, et al. An Iron Regulatory Gene Signature Predicts Outcome in  
608 Breast Cancer. *Cancer Research*. 2011; 71(21): 6728–6737.
- 609 [25] Lausen B, Schumacher M. Maximally Selected Rank Statistics. *Biometrics*. 1992; 48(1): 73.
- 610 [26] Rosenwald A, Wright G, Wiestner A, et al. The proliferation gene expression signature is a  
611 quantitative integrator of oncogenic events that predicts survival in mantle cell lymphoma.  
612 *Cancer Cell*. 2003; 3(2): 185–197.
- 613 [27] Herviou L, Kassambara A, Boireau S, et al. PRC2 targeting is a therapeutic strategy for EZ score  
614 defined high-risk multiple myeloma patients and overcome resistance to IMiDs. *Clin Epigenet*.  
615 2018; 10(1): 121.
- 616 [28] Moreaux J, Reme T, Leonard W, et al. Development of Gene Expression-Based Score to Predict  
617 Sensitivity of Multiple Myeloma Cells to DNA Methylation Inhibitors. *Molecular Cancer*  
618 *Therapeutics*. 2012; 11(12): 2685–2692.
- 619 [29] Garcia S, Guirguis AA, Müller S, et al. Pharmacologic Reduction of Mitochondrial Iron Triggers a  
620 Noncanonical BAX/BAK-Dependent Cell Death. *Cancer Discovery*. 2022; 12(3): 774–791.
- 621 [30] Nisbet-Brown E, Olivieri NF, Giardina PJ, et al. Effectiveness and safety of ICL670 in iron-loaded  
622 patients with thalassaemia: a randomised, double-blind, placebo-controlled, dose-escalation  
623 trial. *The Lancet*. 2003; 361(9369): 1597–1602.

- 624 [31] Neufeld EJ. Oral chelators deferasirox and deferiprone for transfusional iron overload in  
625 thalassemia major: new data, new questions. *Blood*. 2006; 107(9): 3436–3441.
- 626 [32] Elalfy MS, Adly AM, Wali Y, et al. Efficacy and safety of a novel combination of two oral chelators  
627 deferasirox/deferiprone over deferoxamine/deferiprone in severely iron overloaded young beta  
628 thalassemia major patients. *Eur J Haematol*. 2015; 95(5): 411–420.
- 629 [33] Tanaka C. Clinical pharmacology of deferasirox. *Clin Pharmacokinet*. 2014; 53(8): 679–694.
- 630 [34] Samara A, Shapira S, Lubin I, et al. Deferasirox induces cyclin D1 degradation and apoptosis in  
631 mantle cell lymphoma in a reactive oxygen species- and GSK3 $\beta$ -dependent mechanism. *Br J*  
632 *Haematol*. 2021; 192(4): 747–760.
- 633 [35] Kim J, Gómez-Pastora J, Weigand M, et al. A Subpopulation of Monocytes in Normal Human Blood  
634 Has Significant Magnetic Susceptibility: Quantification and Potential Implications. *Cytometry A*.  
635 2019; 95(5): 478–487.
- 636 [36] Wang K, Huang X, Di Liberto M, et al. Cell Cycle Dysregulation in Mantle Cell Lymphoma.  
637 *Hematology/Oncology Clinics of North America*. 2020; 34(5): 809–823.
- 638 [37] Palmero I, Holder A, Sinclair AJ, et al. Cyclins D1 and D2 are differentially expressed in human B-  
639 lymphoid cell lines. *Oncogene*. 1993; 8(4): 1049–1054.
- 640 [38] Paull TT, Rogakou EP, Yamazaki V, et al. A critical role for histone H2AX in recruitment of repair  
641 factors to nuclear foci after DNA damage. *Current Biology*. 2000; 10(15): 886–895.
- 642 [39] Li P, Zhou L, Zhao T, et al. Caspase-9: structure, mechanisms and clinical application. *Oncotarget*.  
643 2017; 8(14): 23996–24008.
- 644 [40] Shahar N, Larisch S. Inhibiting the inhibitors: Targeting anti-apoptotic proteins in cancer and  
645 therapy resistance. *Drug Resistance Updates*. 2020; 52: 100712.
- 646 [41] Fraser C, Ryan J, Sarosiek K. BH3 Profiling: A Functional Assay to Measure Apoptotic Priming and  
647 Dependencies. *Methods Mol Biol*. 2019; 1877: 61–76.
- 648 [42] Lin VS, Anderson MA, Huang DCS, et al. Venetoclax for the treatment of mantle cell lymphoma.  
649 *Ann Lymphoma*. 2019; 3: 4–4.
- 650 [43] Sawalha Y, Goyal S, Switchenko JM, et al. A multicenter analysis of the outcomes with venetoclax  
651 in patients with relapsed mantle cell lymphoma. *Blood Advances*. 2023; 7(13): 2983–2993.
- 652 [44] Chandra D, Liu J-W, Tang DG. Early mitochondrial activation and cytochrome c up-regulation  
653 during apoptosis. *J Biol Chem*. 2002; 277(52): 50842–50854.
- 654 [45] Eleftheriadis T, Pissas G, Liakopoulos V, et al. Cytochrome c as a Potentially Clinical Useful Marker  
655 of Mitochondrial and Cellular Damage. *Front Immunol [Internet]*. 2016 [cited 2023 Jul 20];7.
- 656 [46] Miotto G, Rossetto M, Di Paolo ML, et al. Insight into the mechanism of ferroptosis inhibition by  
657 ferrostatin-1. *Redox Biology*. 2020; 28: 101328.

- 658 [47] Zhao Y, Li Y, Zhang R, et al. The Role of Erastin in Ferroptosis and Its Prospects in Cancer Therapy. *OTT*. 2020; Volume 13: 5429–5441.  
659
- 660 [48] Ciechomska IA, Przanowski P, Jackl J, et al. BIX01294, an inhibitor of histone methyltransferase, induces autophagy-dependent differentiation of glioma stem-like cells. *Sci Rep*. 2016; 6(1):  
661 38723.  
662
- 663 [49] Kimura S, Fujita N, Noda T, et al. Chapter 1 Monitoring Autophagy in Mammalian Cultured Cells  
664 through the Dynamics of LC3. *Methods in Enzymology* [Internet]. Elsevier; 2009 [cited 2023 Sep  
665 1]. p. 1–12. Available from: <https://linkinghub.elsevier.com/retrieve/pii/S007668790803601X>.
- 666 [50] Sun K, Li C, Liao S, et al. Ferritinophagy, a form of autophagic ferroptosis: New insights into cancer  
667 treatment. *Front Pharmacol*. 2022; 13: 1043344.
- 668 [51] Lepelletier Y, Camara-Clayette V, Jin H, et al. Prevention of Mantle Lymphoma Tumor  
669 Establishment by Routing Transferrin Receptor toward Lysosomal Compartments. *Cancer  
670 Research*. 2007; 67(3): 1145–1154.
- 671 [52] Hinman A, Holst CR, Latham JC, et al. Vitamin E hydroquinone is an endogenous regulator of  
672 ferroptosis via redox control of 15-lipoxygenase. *PLoS One*. 2018; 13(8): e0201369.
- 673 [53] Mardones P, Rigotti A. Cellular mechanisms of vitamin E uptake: relevance in alpha-tocopherol  
674 metabolism and potential implications for disease. *J Nutr Biochem*. 2004; 15(5): 252–260.
- 675 [54] Mooberry LK, Sabnis NA, Panchoo M, et al. Targeting the SR-B1 Receptor as a Gateway for Cancer  
676 Therapy and Imaging. *Front Pharmacol*. 2016; 7: 466.
- 677 [55] Brown WJ, Warfel J, Greenspan P. Use of Nile red stain in the detection of cholesteryl ester  
678 accumulation in acid lipase-deficient fibroblasts. *Arch Pathol Lab Med*. 1988; 112(3): 295–297.
- 679 [56] Merolle MI, Ahmed M, Nomie K, et al. The B cell receptor signaling pathway in mantle cell  
680 lymphoma. *Oncotarget*. 2018; 9(38): 25332–25341.
- 681 [57] Shen Y, Li X, Dong D, et al. Transferrin receptor 1 in cancer: a new sight for cancer therapy. *Am J  
682 Cancer Res*. 2018; 8(6): 916–931.
- 683 [58] Jun JC, Rathore A, Younas H, et al. Hypoxia-Inducible Factors and Cancer. *Curr Sleep Med Rep*.  
684 2017; 3(1): 1–10.
- 685 [59] Argyriou P, Papageorgiou SG, Panteleon V, et al. Hypoxia-inducible factors in mantle cell  
686 lymphoma: implication for an activated mTORC1→HIF-1 $\alpha$  pathway. *Ann Hematol*. 2011; 90(3):  
687 315–322.
- 688 [60] Peng L, Liu Y, Chen J, et al. APEX1 regulates alternative splicing of key tumorigenesis genes in non-  
689 small-cell lung cancer. *BMC Med Genomics*. 2022; 15(1): 147.
- 690 [61] Xu X-M, Wang C-G, Zhu Y-D, et al. Decreased expression of SLC 39A14 is associated with tumor  
691 aggressiveness and biochemical recurrence of human prostate cancer. *Onco Targets Ther*. 2016;  
692 9: 4197–4205.

- 693 [62] Zhang Y, Wu X, Zhu J, et al. Knockdown of SLC39A14 inhibits glioma progression by promoting  
694 erastin-induced ferroptosis SLC39A14 knockdown inhibits glioma progression. *BMC Cancer*. 2023;  
695 23(1): 1120.
- 696 [63] Samaniego F, Chin J, Iwai K, et al. Molecular characterization of a second iron-responsive element  
697 binding protein, iron regulatory protein 2. Structure, function, and post-translational regulation.  
698 *J Biol Chem*. 1994; 269(49): 30904–30910.
- 699 [64] Khuroya H, Moore JS, Ahmad N, et al. IRP2 as a potential modulator of cell proliferation, apoptosis  
700 and prognosis in nonsmall cell lung cancer. *Eur Respir J*. 2017; 49(4): 1600711.
- 701 [65] Zhu T, Xiao Z, Yuan H, et al. ACO1 and IREB2 downregulation confer poor prognosis and correlate  
702 with autophagy-related ferroptosis and immune infiltration in KIRC. *Front Oncol*. 2022; 12:  
703 929838.
- 704 [66] Yu G, Tseng GC, Yu YP, et al. CSR1 suppresses tumor growth and metastasis of prostate cancer.  
705 *Am J Pathol*. 2006; 168(2): 597–607.
- 706 [67] Jiang L, Hu G, Chen F-F, et al. CSR1 suppresses tumor growth and metastasis of human  
707 hepatocellular carcinoma via inhibition of HPIP. *Eur Rev Med Pharmacol Sci*. 2017; 21(17): 3813–  
708 3820.
- 709 [68] Kim J, You HJ, Youn C. SCARA3 inhibits cell proliferation and EMT through AKT signaling pathway  
710 in lung cancer. *BMC Cancer*. 2022; 22(1): 552.
- 711 [69] Brown CO, Schibler J, Fitzgerald MP, et al. Scavenger receptor class A member 3 (SCARA3) in  
712 disease progression and therapy resistance in multiple myeloma. *Leuk Res*. 2013; 37(8): 963–969.
- 713 [70] Tesfay L, Paul BT, Hegde P, et al. Complementary anti-cancer pathways triggered by inhibition of  
714 sideroflexin 4 in ovarian cancer. *Sci Rep*. 2022; 12(1): 19936.
- 715 [71] Parker JB, Griffin MF, Downer MA, et al. Chelating the valley of death: Deferoxamine’s path from  
716 bench to wound clinic. *Front Med (Lausanne)*. 2023; 10: 1015711.
- 717 [72] Callens C, Coulon S, Naudin J, et al. Targeting iron homeostasis induces cellular differentiation and  
718 synergizes with differentiating agents in acute myeloid leukemia. *J Exp Med*. 2010; 207(4): 731–  
719 750.
- 720 [73] Benadiba J, Rosilio C, Nebout M, et al. Iron chelation: an adjuvant therapy to target metabolism,  
721 growth and survival of murine PTEN-deficient T lymphoma and human T lymphoblastic  
722 leukemia/lymphoma. *Leuk Lymphoma*. 2017; 58(6): 1433–1445.
- 723 [74] Paubelle E, Zylbersztejn F, Alkhaeir S, et al. Deferasirox and vitamin D improves overall survival in  
724 elderly patients with acute myeloid leukemia after demethylating agents failure. *PLoS One*. 2013;  
725 8(6): e65998.
- 726 [75] Choi JG, Kim J-L, Park J, et al. Effects of oral iron chelator deferasirox on human malignant  
727 lymphoma cells. *Korean J Hematol*. 2012; 47(3): 194–201.

- 728 [76] Lui GYL, Obeidy P, Ford SJ, et al. The iron chelator, deferasirox, as a novel strategy for cancer  
729 treatment: oral activity against human lung tumor xenografts and molecular mechanism of  
730 action. *Mol Pharmacol*. 2013; 83(1): 179–190.
- 731 [77] Kamihara Y, Takada K, Sato T, et al. The iron chelator deferasirox induces apoptosis by targeting  
732 oncogenic Pyk2/ $\beta$ -catenin signaling in human multiple myeloma. *Oncotarget*. 2016; 7(39): 64330–  
733 64341.
- 734 [78] Shinoda S, Kaino S, Amano S, et al. Deferasirox, an oral iron chelator, with gemcitabine  
735 synergistically inhibits pancreatic cancer cell growth in vitro and in vivo. *Oncotarget*. 2018; 9(47):  
736 28434–28444.
- 737 [79] Scoglio M, Cappellini MD, D’Angelo E, et al. Kidney Tubular Damage Secondary to Deferasirox:  
738 Systematic Literature Review. *Children (Basel)*. 2021; 8(12): 1104.
- 739 [80] Towerman AS, Guilliams KP, Guerriero R, et al. Hyperammonemia and acute liver failure  
740 associated with deferasirox in two adolescents with sickle cell disease. *Br J Haematol*. 2023;  
741 201(4): e30–e33.
- 742 [81] Fraser J, Brook R, He T, et al. Deferasirox-induced liver injury and Fanconi syndrome in a beta-  
743 thalassemia major male. *BMJ Case Rep*. 2020; 13(7): e234542.
- 744 [82] Huang W-F, Chou H-C, Tsai Y-W, et al. Safety of deferasirox: a retrospective cohort study on the  
745 risks of gastrointestinal, liver and renal events. *Pharmacoepidemiol Drug Saf*. 2014; 23(11): 1176–  
746 1182.
- 747 [83] Teh MR, Frost JN, Armitage AE, et al. Analysis of Iron and Iron-Interacting Protein Dynamics During  
748 T-Cell Activation. *Front Immunol*. 2021; 12: 714613.
- 749 [84] Tiemann M, Schrader C, Klapper W, et al. Histopathology, cell proliferation indices and clinical  
750 outcome in 304 patients with mantle cell lymphoma (MCL): a clinicopathological study from the  
751 European MCL Network. *Br J Haematol*. 2005; 131(1): 29–38.
- 752 [85] Hoster E, Rosenwald A, Berger F, et al. Prognostic Value of Ki-67 Index, Cytology, and Growth  
753 Pattern in Mantle-Cell Lymphoma: Results From Randomized Trials of the European Mantle Cell  
754 Lymphoma Network. *J Clin Oncol*. 2016; 34(12): 1386–1394.
- 755 [86] Grootjans J, Kaser A, Kaufman RJ, et al. The unfolded protein response in immunity and  
756 inflammation. *Nat Rev Immunol*. 2016; 16(8): 469–484.
- 757 [87] Nordström L, Sernbo S, Eden P, et al. SOX11 and TP53 add prognostic information to MIPI in a  
758 homogenously treated cohort of mantle cell lymphoma--a Nordic Lymphoma Group study. *Br J*  
759 *Haematol*. 2014; 166(1): 98–108.
- 760 [88] Rodrigues JM, Hassan M, Freiburghaus C, et al. p53 is associated with high-risk and pinpoints TP53  
761 missense mutations in mantle cell lymphoma. *Br J Haematol*. 2020; 191(5): 796–805.
- 762 [89] Willis SN, Chen L, Dewson G, et al. Proapoptotic Bak is sequestered by Mcl-1 and Bcl-xL, but not  
763 Bcl-2, until displaced by BH3-only proteins. *Genes Dev*. 2005; 19(11): 1294–1305.

764 [90] Ovejero S, Kumanski S, Soulet C, et al. A sterol-PI(4)P exchanger modulates the Tel1/ATM axis of  
765 the DNA damage response. *EMBO J.* 2023; 42(15): e112684.

766 [91] Han D, Lerner AG, Vande Walle L, et al. IRE1alpha kinase activation modes control alternate  
767 endoribonuclease outputs to determine divergent cell fates. *Cell.* 2009; 138(3): 562–575.

768 [92] Xu X, Liu J, Huang B, et al. Reduced response of IRE1 $\alpha$ /Xbp-1 signaling pathway to bortezomib  
769 contributes to drug resistance in multiple myeloma cells. *Tumori.* 2017; 103(3): 261–267.

770 [93] Wang XZ, Harding HP, Zhang Y, et al. Cloning of mammalian Ire1 reveals diversity in the ER stress  
771 responses. *EMBO J.* 1998; 17(19): 5708–5717.

772 [94] Lee A-H, Iwakoshi NN, Glimcher LH. XBP-1 regulates a subset of endoplasmic reticulum resident  
773 chaperone genes in the unfolded protein response. *Mol Cell Biol.* 2003; 23(21): 7448–7459.

774 [95] Zeeshan H, Lee G, Kim H-R, et al. Endoplasmic Reticulum Stress and Associated ROS. *IJMS.* 2016;  
775 17(3): 327.

776 [96] Moncan M, Mnich K, Blomme A, et al. Regulation of lipid metabolism by the unfolded protein  
777 response. *J Cell Mol Med.* 2021; 25(3): 1359–1370.

778 [97] Han J, Kaufman RJ. The role of ER stress in lipid metabolism and lipotoxicity. *J Lipid Res.* 2016;  
779 57(8): 1329–1338.

780 [98] Rule S, Dreyling M, Goy A, et al. Ibrutinib for the treatment of relapsed/refractory mantle cell  
781 lymphoma: extended 3.5-year follow up from a pooled analysis. *Haematologica.* 2019; 104(5):  
782 e211–e214.

783 [99] Wang ML, Jurczak W, Jerkeman M, et al. Ibrutinib plus Bendamustine and Rituximab in Untreated  
784 Mantle-Cell Lymphoma. *N Engl J Med.* 2022; 386(26): 2482–2494.

785 [100] Giné E, de la Cruz F, Jiménez Ubieta A, et al. Ibrutinib in Combination With Rituximab for Indolent  
786 Clinical Forms of Mantle Cell Lymphoma (IMCL-2015): A Multicenter, Open-Label, Single-Arm,  
787 Phase II Trial. *J Clin Oncol.* 2022; 40(11): 1196–1205.

788 [101] Tivey A, Shotton R, Eyre TA, et al. Ibrutinib as first-line therapy for mantle cell lymphoma:  
789 a multicenter, real-world UK study. *Blood Adv.* 2024; 8(5): 1209–1219.

790 [102] Dreyling M, Doorduijn J, Giné E, et al. Ibrutinib combined with immunochemotherapy with or  
791 without autologous stem-cell transplantation versus immunochemotherapy and autologous  
792 stem-cell transplantation in previously untreated patients with mantle cell lymphoma  
793 (TRIANGLE): a three-arm, randomised, open-label, phase 3 superiority trial of the European  
794 Mantle Cell Lymphoma Network. *Lancet.* 2024; 403(10441): 2293–2306.

795 [103] George B, Chowdhury SM, Hart A, et al. Ibrutinib Resistance Mechanisms and Treatment  
796 Strategies for B-Cell Lymphomas. *Cancers (Basel).* 2020; 12(5): 1328.

797 [104] Decombis S, Bellanger C, Le Bris Y, et al. CARD11 gain of function upregulates BCL2A1 expression  
798 and promotes resistance to targeted therapies combination in B-cell lymphoma. *Blood*. 2023;  
799 142(18): 1543–1555.

800 [105] Agarwal R, Chan Y-C, Tam CS, et al. Dynamic molecular monitoring reveals that SWI–SNF  
801 mutations mediate resistance to ibrutinib plus venetoclax in mantle cell lymphoma. *Nat Med*.  
802 2019; 25(1): 119–129.

803

804

## 805 **Figure Legends**

806

807 **Figure 1. The iron score predicts the clinical outcome in MCL. (A)** A list of 63 genes involved in the  
808 regulation of iron biology was established using previously published data [20,24]. Gene expression  
809 microarray data from one cohort (Staudt cohort) of 71 newly-diagnosed MCL patients was used (accession  
810 number GSE10793). Data were analyzed with Microarray Suite version 5.0 (MAS 5.0), using Affymetrix  
811 default analysis settings and global scaling as normalization method. The trimmed mean target intensity  
812 of each array was arbitrarily set to 500. 4 iron-related genes were found to have a good prognostic value  
813 (in green) and 4 a bad prognostic value (in red). *ABCG2* (ATP-binding cassette transporter G2), *SCARA3*  
814 (Scavenger Receptor Class A Member 3), *IREB2* (Iron Responsive Element Binding Protein 2) and *SFXN4*  
815 (sideroflexin 4); *APEX1* (DNA-(apurinic or apyrimidinic site) lyase), *TFRC* (Transferrin Receptor Protein 1),  
816 *SLC39A14* (Solute Carrier Family 39 Member 14), and *HIF1A* (Hypoxia inducible factor A 1). Scheme was  
817 created with BioRender. **(B)** Patients of the Staudt cohort GSE10793 (n = 71) were ranked according to  
818 increased iron score and a maximum difference in OS (overall survival) was obtained with iron score of -  
819 3.7798 (also named ‘cut point’) splitting patients into high-risk and low-risk groups. The iron score was  
820 significantly associated with high-risk in MCL patients. **(C)** Primary MCL cells from 9 patients were treated  
821 with ironomycin at the indicated concentrations for 4 days. Tumor cells were analyzed by flow cytometry  
822 and expressed in % of control. Results represent the median ± IQR. Statistical significance was tested using  
823 paired t-test: \*\*\* p value < 0.001, \*\*\*\* p value < 0.0001. **(D,E)** Peripheral blood mononucleated cells  
824 (PBMC) from healthy donors (n = 5) were treated with ironomycin or deferasirox for 4 days, counted in  
825 presence of trypan blue to visually distinguish dead cells (trypan blue positive) from living cells (trypan  
826 blue negative). (D) Viability was calculated as the percentage of living cells to total cells (living + dead) in  
827 each condition compared to control. (E) Populations of B-lymphocytes, T-lymphocytes and monocytes  
828 were quantified by flow cytometry and compared to control condition. The 3 populations are expressed  
829 as % of control. Asterisks indicate significant differences compared to control conditions after applying a  
830 Student’s t-test for pairs. \*: p-value < 0.05; \*\*: p-value < 0.01; \*\*\*: p: value < 0.001; ns: not significant.

831 **Figure 2. Ironomycin impairs the proliferation of MCL cells. (A)** JEKO1, JVM2 and MAVER1 cell lines were  
832 treated as indicated for 48 h. Cells were counted at day 0 and at the end of the treatments, and the  
833 number of cells was normalized to day 0 to calculate the proliferation rate. Graphs show the average and  
834 standard deviation of 3-4 independent experiments. **(B)** Cells were treated or not with ironomycin (JEKO1:  
835 10 and 50 nM; JVM2/MAVER1: 50 and 250 nM) and Deferasirox (80 µM) for 48 h and BrdU (10 µg/ml) was  
836 added during the last 1.5 h of treatment. Cells were fixed and processed to detect BrdU incorporation and  
837 total DNA. BrdU+ cells were assigned to S-phase. BrdU- cells were assigned to G0/G1 or G2/M phases



838 based on their DNA content. Results are the mean of 3-4 independent experiments. **(C,D)** Cells were  
839 treated as indicated for 48 h, and the levels of Cyclin D1 and Cyclin D2 were analyzed in cell lysates by  
840 western blot. Tubulin was used as loading control. Figures show 1 representative experiment out of 3. **(E)**  
841 Total mRNA was extracted from cells treated as indicated for 48 h, subjected to retrotranscription and the  
842 levels of expression of *CCND1*, *CCND2*, *RB1* and *CDK4* genes were quantified by qPCR. Graphs show the  
843 average  $\pm$  SD of 3 independent experiments. **(F)** Cells were treated or not with ironomycin (JEKO1: 50 nM;  
844 JVM2/MAVER1: 250 nM) for 48 h, collected and the indicated proteins were analyzed by western blot in  
845 whole cell lysates. In all the graphs in this figure, asterisks indicate significant differences compared to  
846 control conditions after applying a Student's t-test for pairs. \*: p-value < 0.05; \*\*: p-value < 0.01; \*\*\*: p-  
847 value < 0.001; ns: not significant.

848 **Figure 3. (A)** Cells were treated as indicated for 48 h and Annexin V was detected by flow cytometry.  
849 Results are the mean  $\pm$  SD of 3 independent experiments. **(B)** Cells were treated as in (A). The levels of the  
850 indicated proteins were analyzed by western blot. Figure shows 1 representative out of 3 independent  
851 experiments. **(C)** Cells were treated with ironomycin (JEKO1: 50 nM, JVM2/MAVER1: 250 nM) for 48 h,  
852 and the levels of the indicated proteins were analyzed by western blot. Tubulin was used as a loading  
853 control. Figure shows 1 representative out of 3 independent experiments. **(D)** BH3 profiling of JEKO1,  
854 JVM2 and MAVER1. Cells were treated with ironomycin (JEKO1: 50 nM, JVM2/MAVER1: 250 nM) or DMSO  
855 for 20 h. Then, BH3 mimetics (venetoclax: Bcl2i, AZD-5991: Mcl1i, A-1155463: Bcl-xLi) or vehicle DMSO  
856 (control) were added to the culture medium for 4 h. Annexin V+ cells were detected by flow cytometry.  
857 Graphs represent the difference ( $\Delta$ ) between the percentage of Annexin V+ cells in each condition and in  
858 the control (vehicle DMSO). Results are the mean  $\pm$  SD of 3 independent experiments. **(E)** Cells were pre-  
859 treated with the ferroptosis inhibitor Ferrostatin-1 (10  $\mu$ M, 30 min) before treatment with ironomycin  
860 (JEKO1: 50 nM; JVM2/MAVER1: 250 nM) or the ferroptosis inducer erastin (4  $\mu$ M) for 48 h. Annexin V was  
861 detected by flow cytometry. Graphs show the mean  $\pm$  SD of 3-4 independent experiments. In all the graphs  
862 in this figure, asterisks indicate significant differences compared to control conditions after applying a  
863 Student's t-test for pairs. \*: p-value < 0.05; \*\*: p-value < 0.01; \*\*\*: p-value < 0.001; \*\*\*\*: p-value < 0.0001;  
864 ns: not significant.

865 **Figure 4. Ironomycin downregulates the expression of BCR-related genes and synergizes with BTK**  
866 **inhibitor ibrutinib. (A)** JEKO1, JVM2 and MAVER1 cells were treated with ironomycin (JEKO1: 50 nM;  
867 JVM2/MAVER1: 250 nM) for 48 h. Total RNA was extracted and RNA-sequencing was performed. GSEA  
868 analysis of down- and up-regulated pathways is shown. FDR: false discovery rate. **(B)** Cells were treated  
869 with ironomycin (JEKO1: 50 nM, JVM2/MAVER1: 250 nM) for 48 h, and the levels of the indicated proteins  
870 were analyzed by western blot. Tubulin was used as a loading control. Figure shows 1 representative out  
871 of 3 independent experiments. **(C-E)** Cells were seeded in flat-bottom 96-well plates, treated with  
872 increasing concentrations of ironomycin (1 – 4000 nM) and ibrutinib (0.125 – 32  $\mu$ M), and incubated for  
873 4 days. Cell growth was assessed by CellTiter Glo<sup>®</sup> assay. Drug synergy was calculated using R package  
874 “SynergyFinder”. Effect of drug combination on cell growth is shown in a pseudo-color scale from red  
875 (synergism) to green (antagonism). Matrixes show the mean of 3 independent experiments.

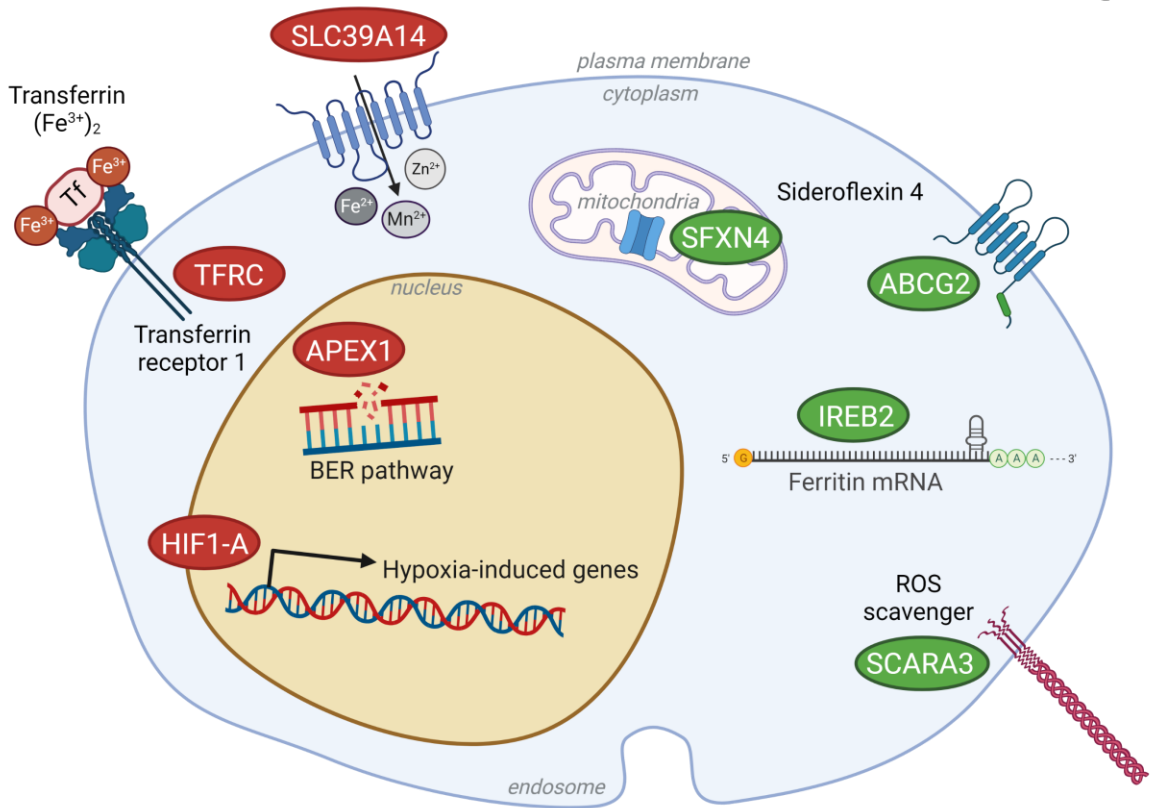
876 **Figure 5. (A)** JEKO1, JVM2 and MAVER1 cell lines were treated as indicated with ironomycin (JEKO1: 50  
877 nM; JVM2/MAVER1: 250 nM) and ibrutinib (JEKO1: 0.5  $\mu$ M; JVM2: 1.5  $\mu$ M; MAVER1: 6.25  $\mu$ M) for 48 h.  
878 Cells were counted at day 0 and at the end of the treatments, and the number of cells was normalized to  
879 day 0 to calculate the proliferation rate. Graphs show the mean  $\pm$  SD of 3 independent experiments. **(B)**  
880 Cells were treated as in (A) and BrdU (10  $\mu$ g/ml) was added during the last 1.5 h of treatment. Cells were

881 fixed and processed to detect BrdU incorporation and total DNA. BrdU+ cells were assigned to S-phase.  
882 BrdU- cells were assigned to G0/G1 or G2/M phases based on their DNA content. Results are the mean  $\pm$   
883 SD of 3-4 independent experiments. **(C)** Cells were treated as in (A) and Annexin V was detected by flow  
884 cytometry. Graphs show the mean  $\pm$  SD of 3-4 independent experiments. (A-C) Asterisks indicate a  
885 significant difference compared to control conditions after applying a Student's t-test for pairs. \*: p-value  
886 < 0.05; \*\*: p-value < 0.01; \*\*\*: p-value < 0.001; \*\*\*\*: p-value < 0.0001; ns: not significant. **(D)** Cells were  
887 treated as in (A). Total RNA was extracted, RNA-sequencing was performed and GSEA analysis was applied  
888 to find upregulated and downregulated pathways in cells treated with ironomycin plus ibrutinib. FDR:  
889 false discovery rate.

890 **Figure 6.** Model of ironomycin cytotoxic effects alone and in combination with other drugs. **(A)** Ironomycin  
891 sequesters iron in lysosomes triggering different cellular responses: (1) the production of ROS through the  
892 Fenton reaction that cause peroxidation of lipids, which require GPX4 activity to be detoxified, and DNA  
893 damage that will cause cell cycle arrest; (2) impairment of mitochondrial metabolism and ATP production;  
894 (3) ER stress characterized by the activation of UPR, notably the IRE1 $\alpha$  signaling pathway. High levels of  
895 lipid peroxidation, DNA damage, mitochondrial activity impairment and sustained ER stress lead to  
896 ferroptosis and apoptosis. Combination of ironomycin with BH3 mimetics have a synergistic toxic effect  
897 in MCL cells. **(B)** Ironomycin downregulates BCR-signaling and synergizes with ibrutinib. Combination of  
898 both drugs further increases a sustained UPR that leads to apoptosis. Figures were created with  
899 Biorender.com.

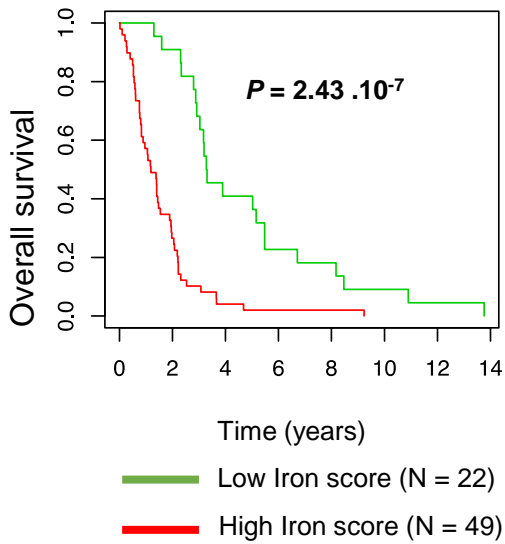
900

**A**

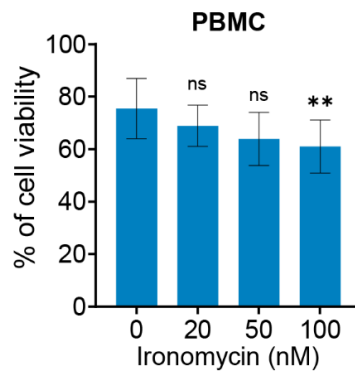


**B**

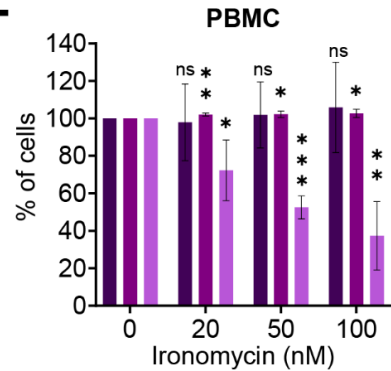
Staudt cohort (N = 71)



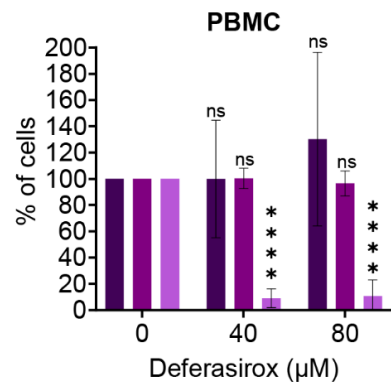
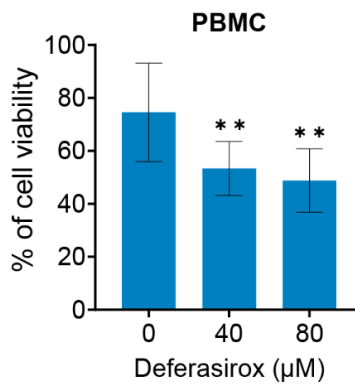
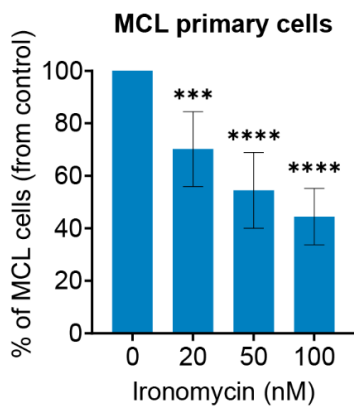
**D**



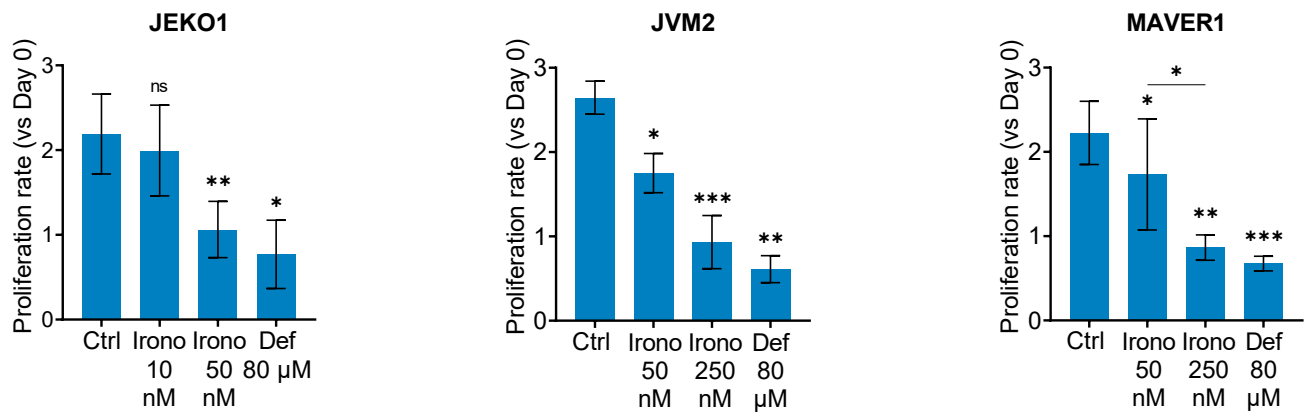
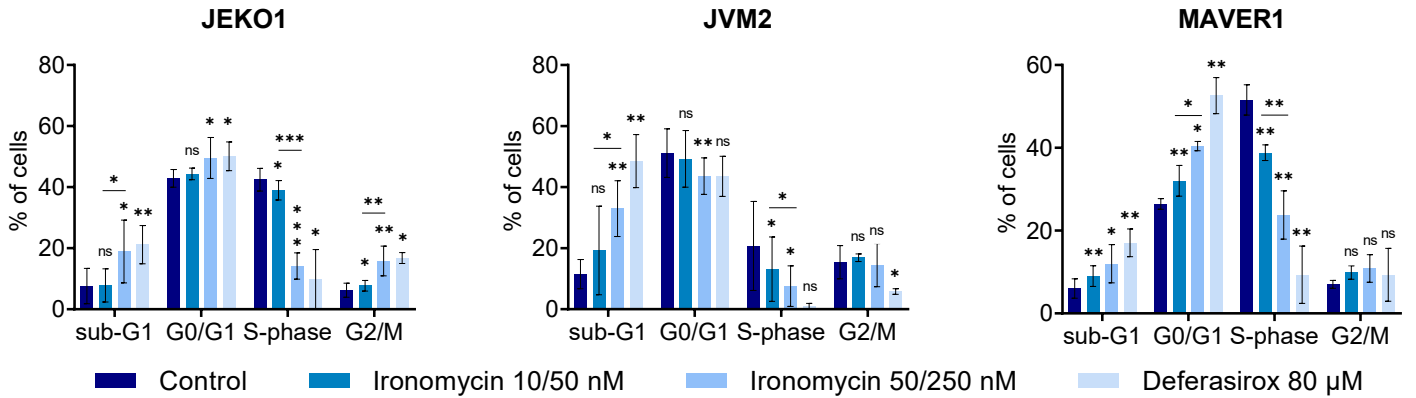
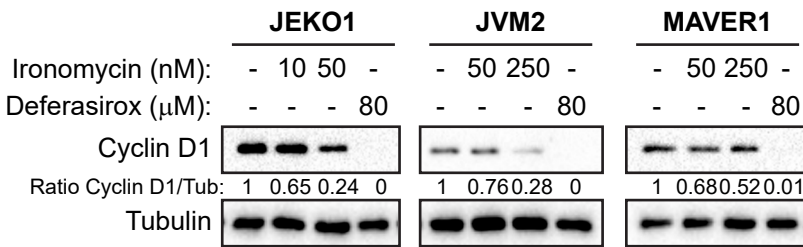
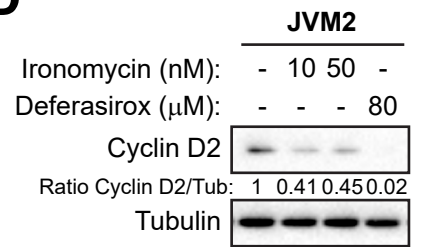
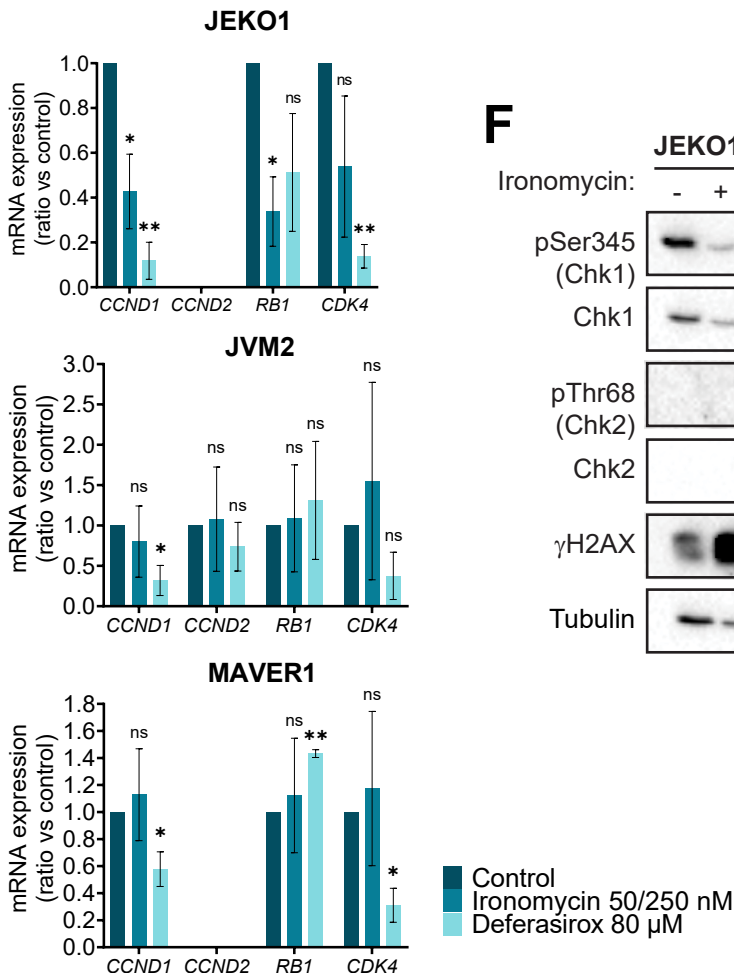
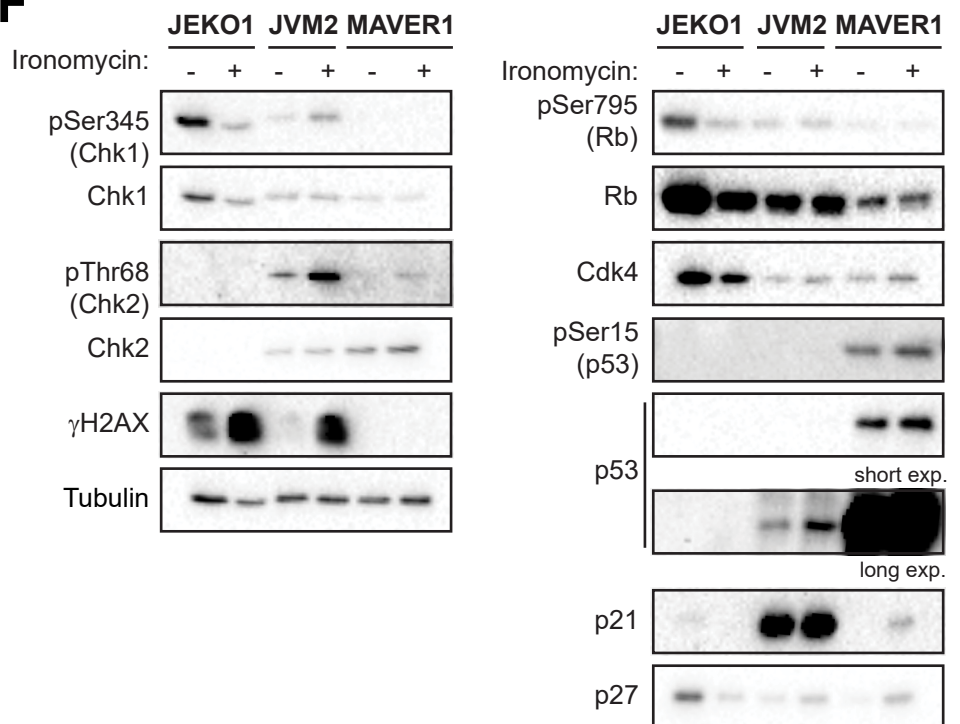
**E**



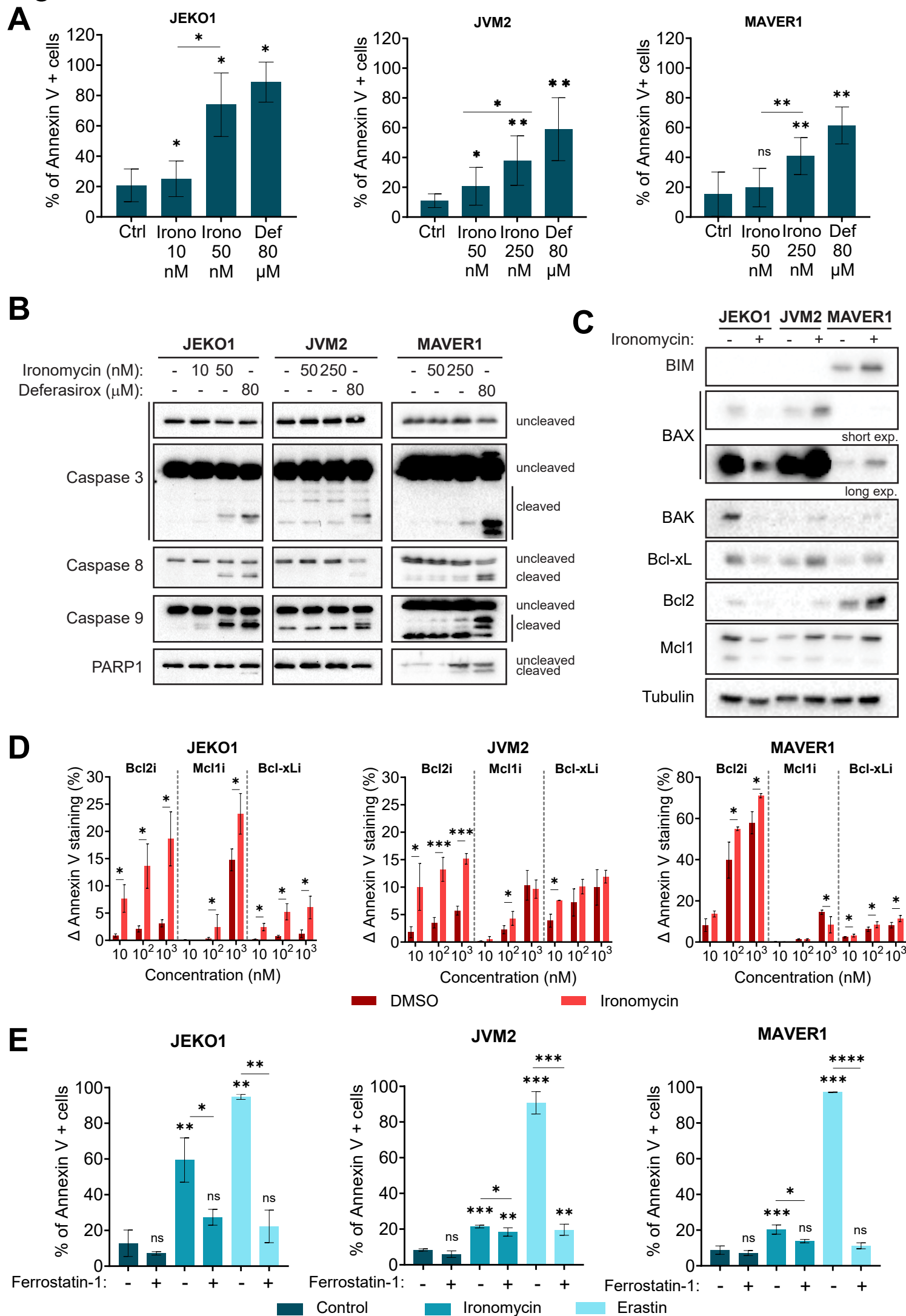
**C**



■ B Lymphocytes  
 ■ T Lymphocytes  
 ■ Monocytes

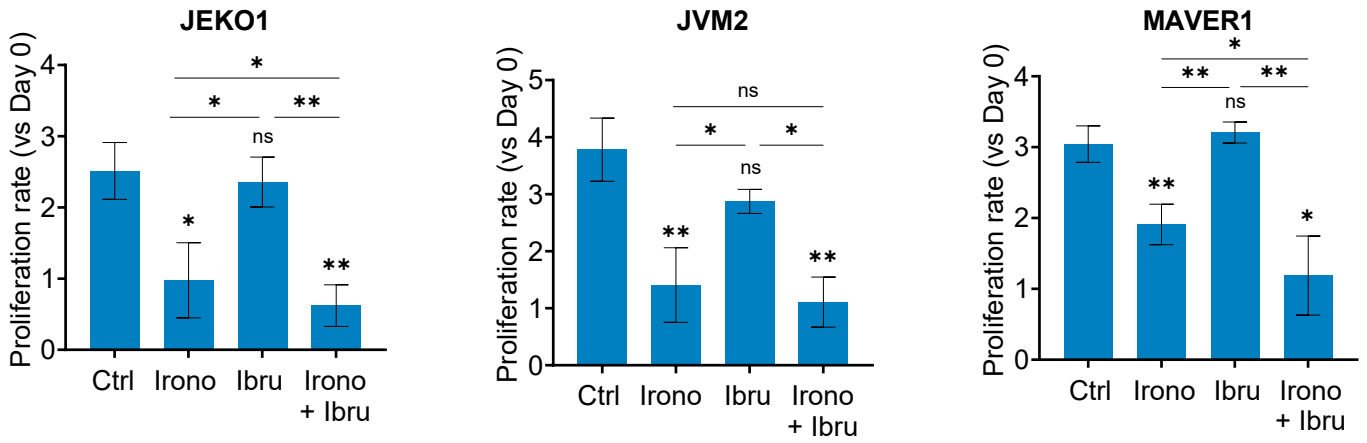
**Figure 2****A****B****C****D****E****F**

# Figure 3

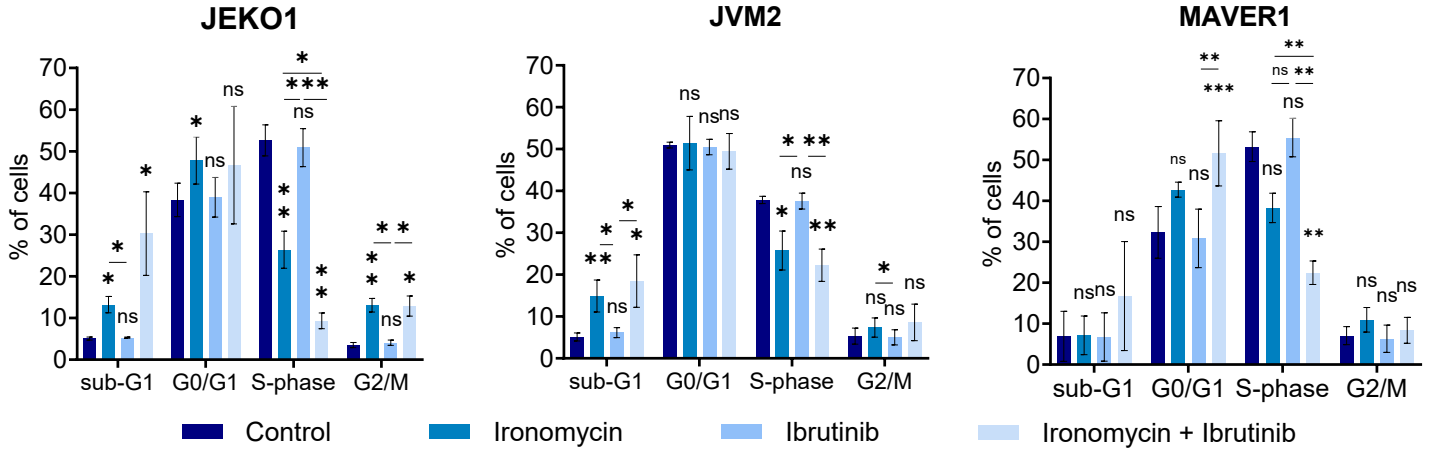




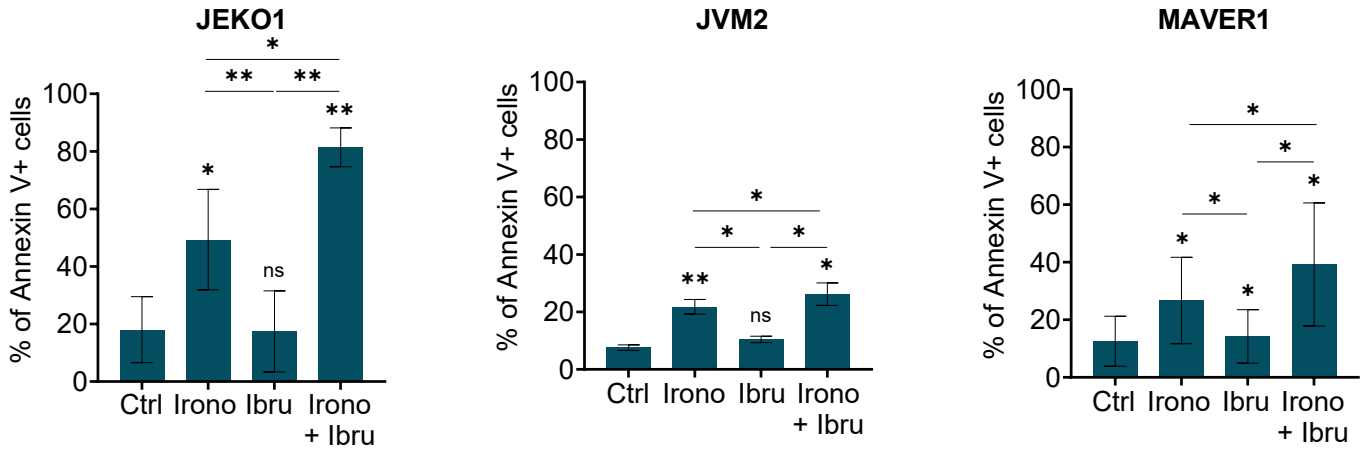
**A**



**B**



**C**



**D**

**GSEA: Upregulated in Ironomycin + Ibrutinib**

**GSEA: Downregulated in Ironomycin + Ibrutinib**

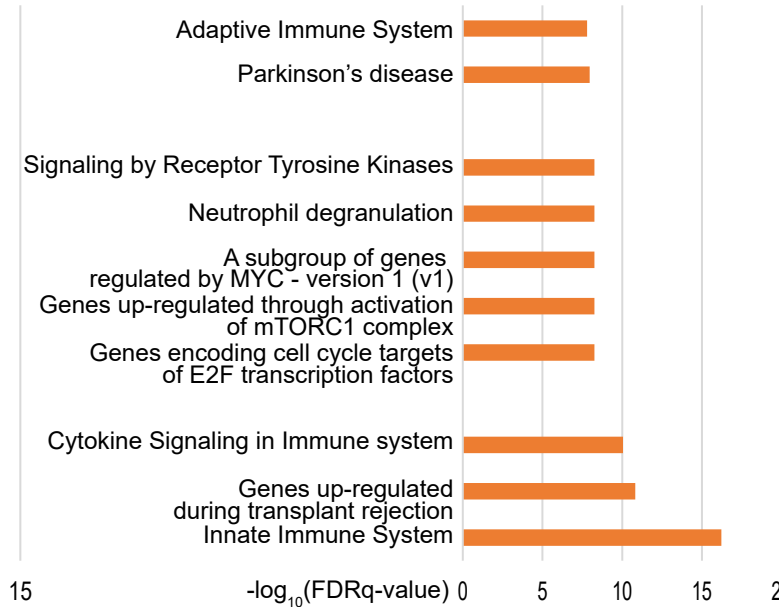
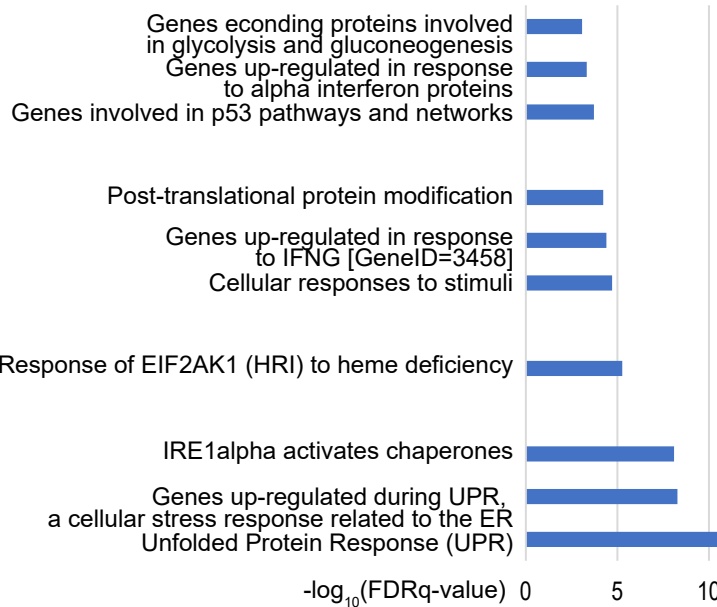
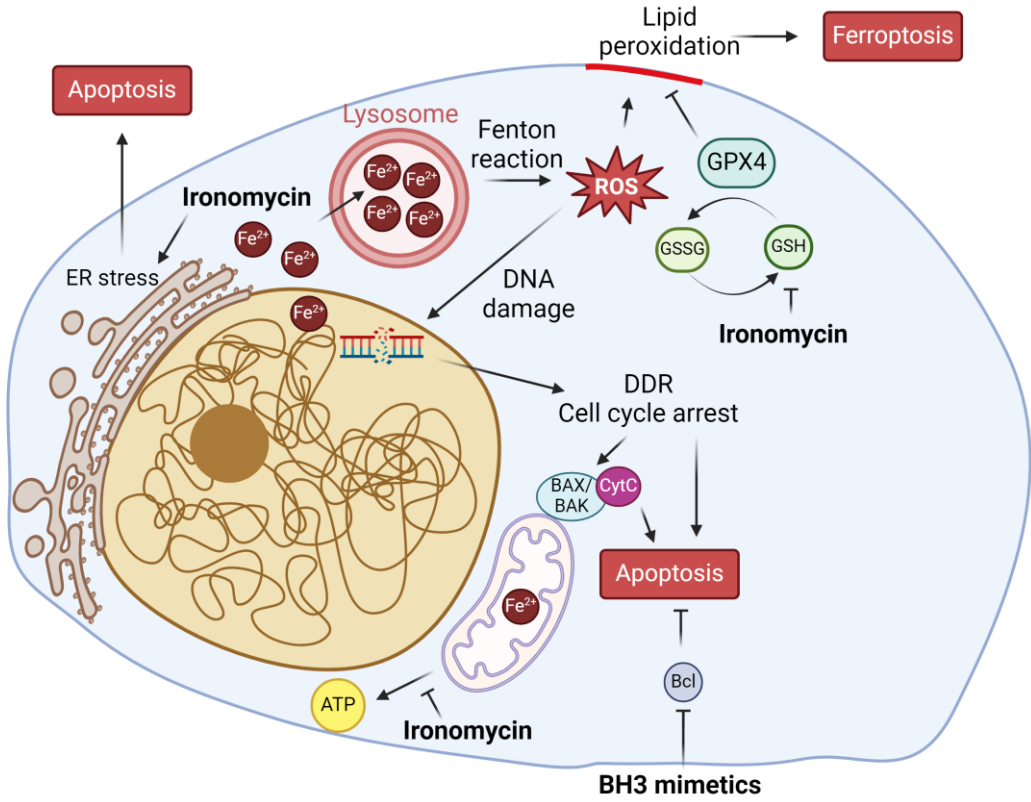




# Figure 6

## A



## B

